AD_____

Award Number: DAMD17-99-1-9404

TITLE: Opto-Acoustic Tomography for Early Detection of Breast Cancer

PRINCIPAL INVESTIGATOR: Alexander A. Oraevsky, Ph.D.

CONTRACTING ORGANIZATION: The University of Texas
Medical Branch at Galveston
Galveston, Texas 77555-0136

REPORT DATE: September 2000

TYPE OF REPORT: Annual

PREPARED FOR: U.S. Army Medical Research and Materiel Command
Fort Detrick, Maryland 21702-5012

REPORT DOCUMENTATION PAGE

Form Approved
OMB No. 074-0188

1. AGENCY USE ONLY (Leave blank)	2. REPORT DATE	3. REPORT TYPE AND DATES COVERED
	September 2000	Annual (1 Sep 99 - 31 Aug 00)

4. TITLE AND SUBTITLE

Opto-Acoustic Tomography for Early Detection of Breast Cancer

5. FUNDING NUMBERS

DAMD17-99-1-9404

6. AUTHOR(S)

Alexander A. Oraevsky, Ph.D.

7. PERFORMING ORGANIZATION NAME(S) AND ADDRESS(ES)

The University of Texas Medical Branch at Galveston

Galveston, Texas 77555-0136

E-MAIL: alexander.oraevsky@utmb.edu

8. PERFORMING ORGANIZATION REPORT NUMBER

9. SPONSORING / MONITORING AGENCY NAME(S) AND ADDRESS(ES)

U.S. Army Medical Research and Materiel Command
Fort Detrick, Maryland 21702-5012

10. SPONSORING / MONITORING AGENCY REPORT NUMBER

11. SUPPLEMENTARY NOTES

12a. DISTRIBUTION / AVAILABILITY STATEMENT

Approved for public release; distribution unlimited

12b. DISTRIBUTION CODE

13. ABSTRACT ***(Maximum 200 Words)***

The main goal of our USAMRMC project was to develop a new concept in diagnostic imaging of breast cancer, laser optoacoustic imaging system (LOIS). The major effort during the Year-1 project was made on system modeling, design, and fabrication of system hardware and development of the system software. The test results demonstrated that utilization of optical tissue contrast produces significant advance in quality of ultrasound images. All research aims were accomplished yielding a clinical prototype of two-dimensional optoacoustic imaging system with parameters exceeding those of existing ultrasound systems: tissue contrast 250-600%, sensitivity 5 V/bar, effective noise 4 μbar, and resolution of 0.5 mm x 1 mm. After thorough tests in gel phantoms resembling optical and acoustic properties of the breast, LOIS performance was evaluated *ex-vivo* in mastectomy specimens with ductal carcinoma. The results demonstrated that LOIS produces high-resolution images with significantly enhanced contrast between tumors and normal tissues yielding resolution similar to that of digital ultrasound imaging.

14. SUBJECT TERMS

Breast Cancer, tumor angiogenesis, imaging, diagnostics

15. NUMBER OF PAGES

46

16. PRICE CODE

17. SECURITY CLASSIFICATION OF REPORT	18. SECURITY CLASSIFICATION OF THIS PAGE	19. SECURITY CLASSIFICATION OF ABSTRACT	20. LIMITATION OF ABSTRACT
Unclassified	Unclassified	Unclassified	Unlimited

NSN 7540-01-280-5500

Standard Form 298 (Rev. 2-89)
Prescribed by ANSI Std. Z39-18
298-102

Table of Contents

ANNUAL REPORT 2000

(4) INTRODUCTION

The subject of our project is diagnostic imaging of breast tumors. We are testing hypothesis that prevailing absorption of short laser pulses in tumors due to advanced angiogenesis compared with optical absorption in normal tissues will generate pressure profiles in breast tumors and convert these tumors into acoustic sources. Ultrasonic waves deliver diagnostic information to the breast surface, where signals are detected by piezoelectric transducers. Reconstruction of two-dimensional images of breast sectors is made on the basis of time-resolved detection and analysis of wide-band ultrasound profiles recorded with a linear array transducer located at the breast surface. Opto-acoustic tomography takes advantage of a well-developed signal processing and image reconstruction algorithms, currently employed in wide-band ultrasonography.

The purpose of this project is to incorporate laser excitation into a wide-band ultrasonography system (with a linear array probe) to yield a clinical prototype Laser Optoacoustic Imaging System (LOIS) and test this system initially in blood perfused phantoms and then in breast cancer patients. The tissue phantoms will be designed to resemble natural optical and acoustic properties of breast with advanced angiogenesis. Racial differences, such as light absorption properties of various skin types will also be accounted for. Experiments in blood perfused phantoms will test the hypothesis that the breast circulation system and angiogenesis can be visualized with high sensitivity and contrast. Clinical studies should confirm our hypothesis that the breast structural heterogeneity will not compromise the optoacoustic image quality, or may be accounted for in the optoacoustic image processing.

The major anticipated advantages of the laser optoacoustic tomography are listed in a sequence corresponding to their importance: (1) high optical contrast between tumors and normal tissues which results from enhanced density of the microcirculation network within and around tumors and enhanced concentration of other endogenous chromophores in cancer cells; (2) high sensitivity of detection which results from efficient opto-thermal generation of pressure in tumors, and sensitive detection of ultrasonic waves with novel piezoelectric transducers; (3) high (<1 mm) spatial resolution which results from pulsed laser excitation and time-resolved detection of undistorted ultrasonic wave profiles with array detectors; (4) substantial depth of monitoring (up to 8-cm) which results from deep penetration of the near-infra-red photons in tissues, efficient conversion of laser energy into ultrasonic waves propagating through the breast with insignificant attenuation and minimal distortion, and from high sensitivity (5 V/bar) of piezoelectric transducers; and (5) applicability to dense breasts.

(5) BODY OF REPORT

During the Year-1 project period all specific aims and milestones were accomplished. Specific details of the optoacoustic imaging system development and tests are presented below.

Task 1 (Year 1): Development and fabrication of a clinical laser optoacoustic imaging system (LOIS) on the basis of commercially available components of a digital ultrasound imaging system, such as HDI-1000 from ATL.

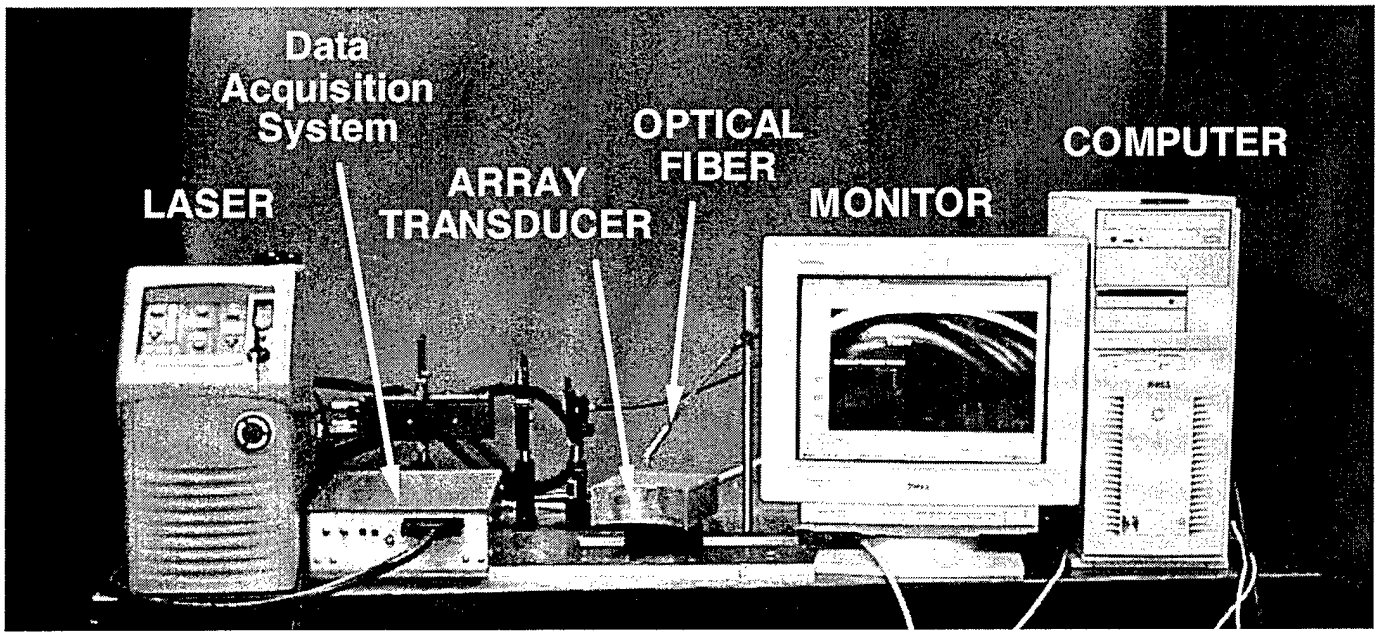

Figure 1. Photograph of a clinical laser opto-acoustic imaging system LOIS-2.

Milestones of Task 1 were accomplished.

1a. By the end of the first quarter a compact nanosecond laser was incorporated in the optoacoustic imaging system. The system is made flexible to utilize either an Nd:YAG laser (Big Sky Lasers, Inc. Boseman MT) or Alexandrite laser (CEO Inc., Orlando FL). An HDI-1000 ultrasound imaging system from ATL Inc. (Seatlle, WA) was tested and found not optimal as a prototype for LOIS. Therefore, an electronic registration system with low noise and high dynamic range for fast signal acquisition and storage was developed by LaserSonix Technologies, Inc. (Houston, TX) and provided to our laboratory as a collaborative effort. The electronic system was then fabricated and assembled at the PI's laboratory at UTMB. By the end of the second quarter the system was made operational and tested. Ultrawideband piezoelectric transducer was designed by LaserSonix Technologies, Inc. in collaboration with PI's laboratory and fabricated by Materials Systems Inc. (Littleton, MA). The electronics and software was modified in accordance with the detection system change. Software codes for two dimensional image reconstruction was completed and tested [1].

1b. By the end of the second quarter a software package for automatic system control, signal processing and image reconstruction was developed and tested. Each system component was verified to possess optimal characteristics determined on the basis of preliminary results of our experimental and theoretical studies and work experience with existing bench-top system. The reliability and safety of the system was tested. Theoretical modeling of LOIS yielded satisfactory sensitivity and resolution, so that the clinical Laser Optoacoustic Imaging System (LOIS-2) was completed and prepared for experiments [2].

First experiments with LOIS-2 were performed in gel phantoms simulating dense breast with small tumors simulated by hemoglobin-colored spheres. Two dimensional optoacoustic images displayed position and and diameters of spheres in agreement with their real positions and diameters [3, see Appendix].

Further experiments with opto-acoustic imaging system LOIS-2 aimed at detection of breast carcinoma located deep within a large mass of breast tissue. The experiment performed at UTMB demonstrated potential of LOIS in high contrast imaging of malignant tumors [4,5, see Appendix]. Breast specimens were obtained after radical mastectomy and examined within the first ten minutes after surgical excision. It provided specimens that underwent minimal alterations of tissue optical properties, except some blood was drained form the specimens. After opto-acoustic imaging procedure, pathologist examined the mastectomy specimens in order to determine tumor geometry. Location of tumors was not known prior to opto-acoustic imaging procedure. Opto-acoustic image of breast with carcinoma is presented in Fig. 2.

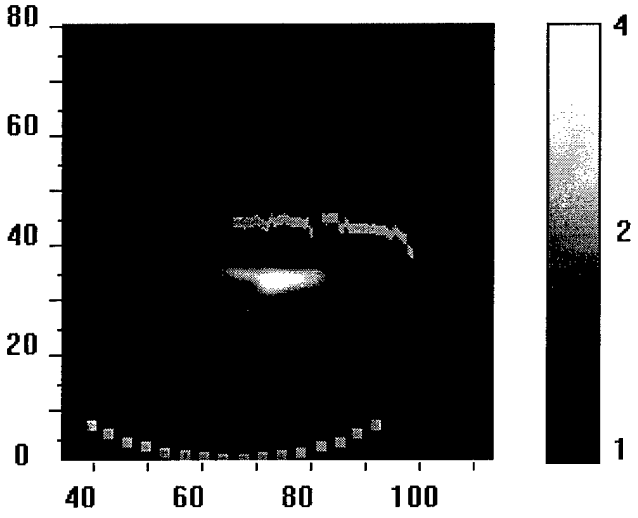

Figure 2. Optoacoustic image of breast cancer patient 408112P. Note that the tumor core and sprouts are visualized with high contrast.

Laser safety of the system was evaluated. The opto-acoustic imaging procedure was performed using laser fluence of 50 mJ/cm^2 which corresponds to half maximum of permissible laser exposure for the skin in the near infrared spectral range, as described in American National Standards for Safe Use of Lasers. The laser irradiance of 50 mJ/cm^2 can induce a temperature rise of only 50-100 mK at the irradiated breast surface and about 0.5-1 mK in tumor located at a 5-cm depth. The laser irradiation was performed with 14-ns laser pulses. Such a short duration of laser pulses ensured that the laser-induced pressure was confined in the target volume of tumor during

laser heating, yileding high resolution and and high efficiency of pressure generation with laser pulses.

Optical fiber was scanned along the surface of the radical mastectomy specimen with 4-mm interval. Sixteen opto-acoustic signals were employed for data collection and subsequent image reconstruction. The scan passed directly over the tumor. The tumor core, horizontal tail and small sprouts may be clearly seen in the opto-acoustic image (confirmed by subsequent pathology examination). The dimension of a tumor core can be estimated as 10x7 mm. Tumor was detected at the depth of 11 mm from the surface. Skin was removed from most part of the specimen, therefore the irradiated surface is depicted as a rough line. Opto-acoustic contrast between the tumor and surrounding normal tissues in this image exceeds 350% making surrounding normal tissue looking dark on the image.

The same breast was imaged in vivo with General Electric mammography system with Mo anode and Mo filter and with Acuson 128 XP/10 system employing 3.5 MHz C3-curved linear array transducer. These images are depicted in Fig. 3. X-ray image revealed all details of this tumor including core with microcalcifications and lateral sprouts. However, x-ray also showed other areas of the breast similarly bright on mammography image, however, found normal. The ultrasound image of the same tumor was not very impressive. The core of tumor and its long tail may also be seen in this image. However, small sprouts are not visible to limited acoustic contrast [5].

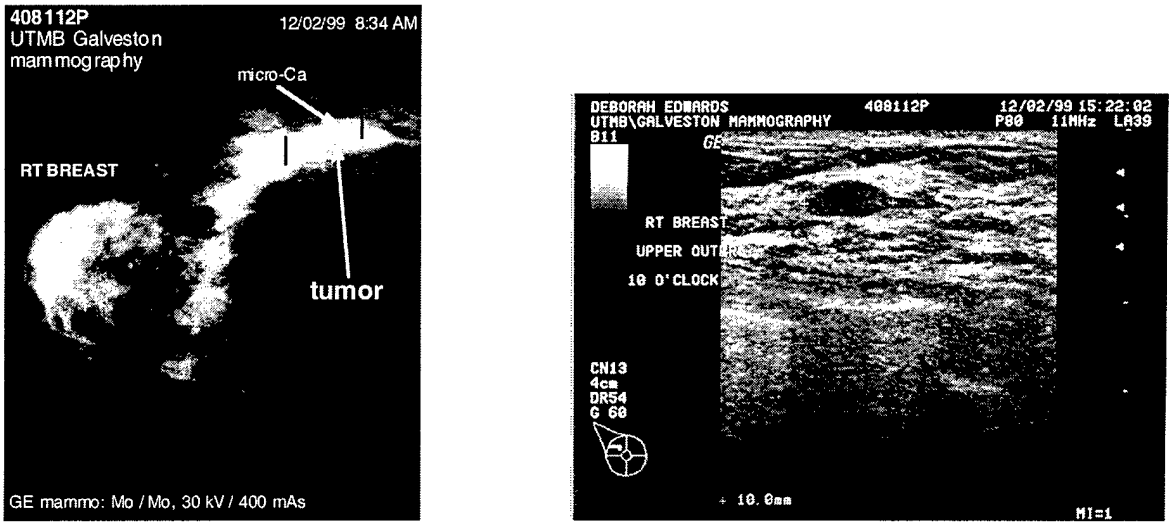

Figure 3. X-ray radiography image obtained *in vivo* with General Eelectric mamography system, Mo anode, Mo filter (right) and ultrasound image obtained with Acuson 128 XP/10 3.5 MHz USI system (left) of a malignant tumor in the breast. UTMB Patient # 408112P. Note that contrast of the tumor relative to background is not sufficient to define exact shape and dimensions of this malignancy.

Using the experimental data obtained, one can calculate minimal radius of spherical tumors with various blood contents, which can currently be detected inside the breast [5-7]. The radius of the minimal detectable spherical tumor is plotted in Fig. 4 as a function of depth from the irradiated surface for various absorption coefficients corresponding to different blood content in tumors. The anticipated blood content in actively growing small tumors is about 4-16% as found in tumor pathology studies.

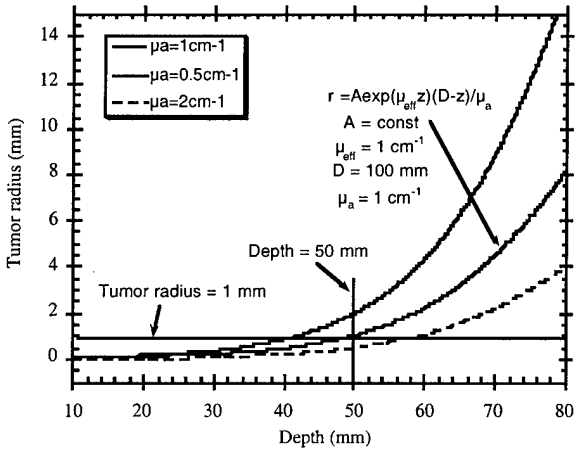

Figure 4. Minimally detectable tumor radius as a function of tumor depth in the bulk of normal tissue.

The areas above the curves in Fig. 4 represent parameters of tumors, which can be detected by wide-band acoustic transducers made of piezoelectric composite materials used in our experiments. The areas under the curves represent areas below the limit of detection for these transducers. Fig. 4 demonstrates that the sensitivity of LOIS-2 permits detection of 2-mm tumors with an average blood content of 8% at a depth of ~6 cm. Therefore, the sensitivity of our current laser optoacoustic imaging system is sufficient for detecting small tumors (with or without calcification) using a safe level of laser irradiation. The limits of detection for laser optoacoustic tomography may be further improved with the use of state-of-the-art acoustic transducer arrays supported by the most advanced electronics and image processing software. This indicates that LOIS has a potential for early detection of breast cancer, which will be tested in later stages of our project.

Task 2 (Year 1): Evaluation of the laser optoacoustic imaging system using tissue phantoms simulating dense breast with advanced tumor angiogenesis.

Milestones of Task 2 were accomplished.

Milestone 2a. By the end of the third quarter the clinical system performance was tested in tissue phantoms resembling optical and mechanical properties of breast with tumor angiogenesis. The clinical system sensitivity, the accuracy of the "tumor" localization, the image contrast and spatial resolution will be compared with the state-of-the-art ultrasound and mammography systems.

Clinical optoacoustic imaging system was assembled and its performance was evaluated in comparison with our current bench-top system using tissue phantoms made of chicken breast slabs and milk-gelatin slabs with embedded blood vessels extracted from mice and rats and operated using closed loop peristaltic pump [4,8,9].

Figurre 5 (a,b) shows two optoacoustic images of a gel phantom with optical properties resembling dense breast with one artery and one vein. Blood vessels surgically extracted from a rat and filled with blood, one with deoxygenated blood and one with oxygenated blood, we embedded inside the gel phantom. A cross-sectional two-dimensional image was made of this tissue phantom. External diameter of blood vessels was approximately 0.72 mm and the lumen diameter was 0.44 mm.

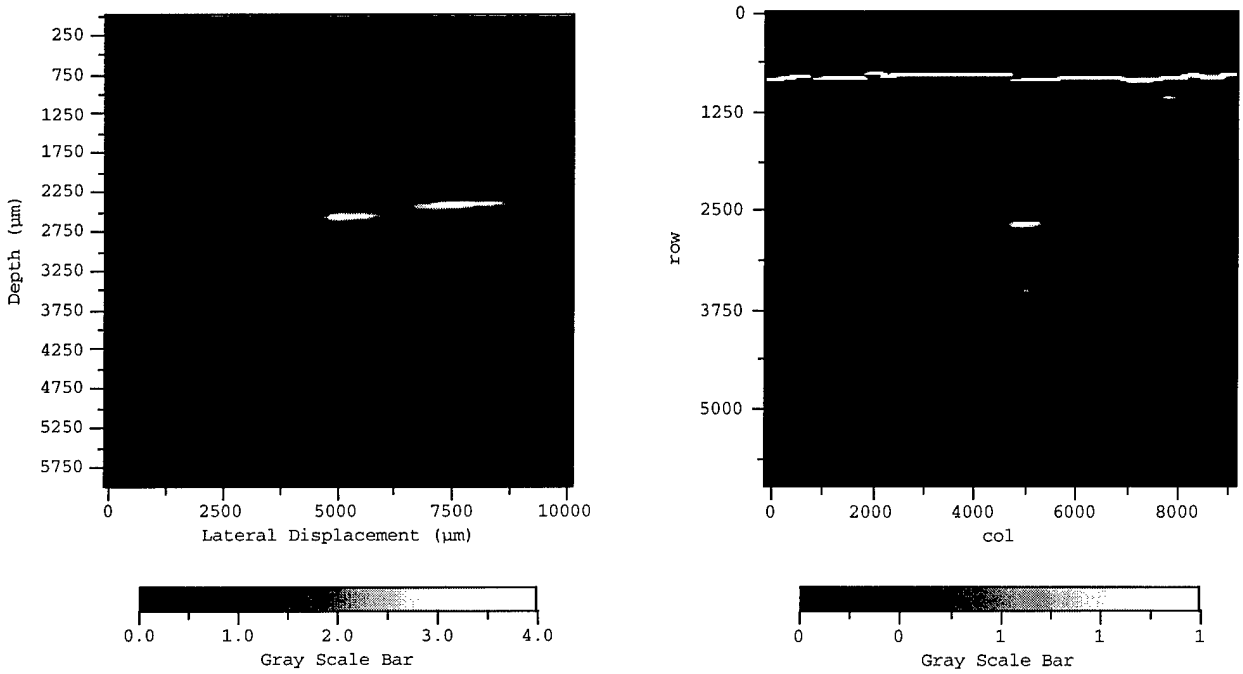

Figure 5. Optoacoustic images of tissue phantoms made of milk gelatin with embedded two blood vessels filled with blood. Imaging was performed with two different laser wavelengths: 532 nm (a) and 1064 nm (b). One blood vessel had oxygen saturation level of hemoglobin equal 70%. The other blood vessel had oxygen saturation level of about 10%.

One can see that images of both blood vessels have equal brightness at the wavelength of 532 nm where oxyhemoglobin and deoxyhemoglobin have similar optical absorption (Fig. 5a), the effect anticipated also at the

wavelength of Alexandrite laser operating at 780 nm. However, at the wavelength of 1064 nm blood vessel with oxygenated arterial blood has much brighter image compared with the blood vessel filled with deoxygenated blood (almost invivible) in Fig. 5b [4,7,8].

The same phantom was imaged with General Electric mammography system anode and filters made of molibdenum and with Acuson 128 XP/10 system employing 3.5 MHz C3-curved linear array transducer. This experiment was designed and performed in order to compare the optoacoustic system sensitivity, the accuracy of the blood vessel localization, the image contrast and spatial resolution with those of the state-of-the-art mammography and ultrasonography systems. However, neither x-ray mammography nor ultrasonography could visualize blood vessels inside dense gelatin phantom. The reason for X-ray system failure is well known and can be explained by high radiologic density of phantom tissue (similar to density of a young woman). The reason for ultrasound failure is the absence of acoustic contrast in density of blood vessels and surrounding gelatin. This experiment reveal potential advantage of optoacoustic imaging system compared with existing modalities.

Milestone 2b. By the end of the fourth quarter the optimal characteristics of each system component from the stand point of diagnostic efficacy, and safety was determined. The system parameters were improved utilizing the results of the preliminary evaluation in tissue phantoms. The changes in the transducer array design suggested by results of *in vitro* studies were incorporated.

Figure 4. Photograph of the linear array of 32 ulrawideband ultrasonic transducers with improved characteristics: sensitivity 5 V/bar, resolution 0.5x1 mm in wide focal zone.

In order to optimize optoacoustic system characteristics form the stand point of diagnostic efficacy, safety, resolution and sensitivity, such laser irradiation parameters as dynamic range and ultrasonic bandwidth of the acoustic detection were varied. Optimal parameters of the array transducer were found to be as follows: (1) ultrasound detection bandwidth: 20 kHz to 4 MHz, dimensions of each transducer 1.5 mm x 1mm with 1 mm gaps, 6 transducers in one piezoelement, 64 piezoelements total in 120^0 linear array with diameter of 120 mm. Sensitivity of such transducer made of PZT-5H ceramic embedded in polymer-epoxy resin with 2-2 structure was exceptionally high, 5 V/bar with effective noise pressure of only 4 μbar [6,10].

(6) KEY ACCOMPLISHMENTS

• Laser Opto-acoustic imaging system (LOIS) was developed and assembled for two-dimensional tomography of early breast cancer utilizing components of wide-band ultrasound imaging system and nanosecond Nd:YAG or Alexandrite lasers.

• LOIS was tested in gelatin phantoms simulating dense breast with blood circulation. Experiments demonstrated that LOIS is capable of not only visualizing blood vessels, but also differentiating veins with deoxygenated blood from arteries with oxygenated blood.

• LOIS was tested in real breast with carcinoma ex-vivo (radical mastectomy specimen). Experiment demonstrated that LOIS can visualize details of malignant tumor not present in ultrasound images.

(7) REPORTABLE OUTCOMES

• Manuscripts: 3 published, 3 in preparation, Abstracts – 4, Presentations acknowledged USAMRMC support – 4.

• Patents: 1 patent application USPTO #60/147,577 submitted on August 6, 2000 entitled: "Opto-Acoustic Monitoring of Blood Oxygenation" (with co-inventors: Rinat Esenaliev, Donald Prough, and Massoud Motamedi).

• Funding applied for based on work supported by this award: USAMRMC Prostate Cancer Program-2000, "Novel imaging system for early detection of prostate cancer", $558,600.

(8) CONLUSIONS

• Laser opto-acoustic imaging system combining pulsed optical excitation of pressure profiles and sensitive ultrawide-band detection of ultrasound is capable of visualizing breast tumors with exceptional contrast relative to normal breast tissue background.

• An evidence based on imaging blood vessels with oxy- and deoxy- blood was obtained that LOIS may be capable of differentiating malignant tumors (with deoxy-blood in tumor angiogenesis) from benign tumors (with oxy- blood in tumor angiogenesis).

• Optimal parameters for clinical LOIS are as follows:

Optical Excitation – 10 ns to 100 ns laser pulses with repetition rate of 10 Hz, fluence of 50 mJ/cm2, and wavelength chosen from the near infrared range between 680 nm and 1064 nm and dependent on the type of tumor to be imaged.

Ultrasonic Detection – piezoelectric transducers made of 2-2 ceramic-polymer composite material operating in an ultrawide band of ultrasonic frequencies from 20 kHz to 4 MHz.

(9) REFERENCES

1. Yu.V. Julina, V.A. Andreev, A.A. Karabutov, A.A. Oraevsky: Filtering and reconstruction of wide-band ultrasound sources in opto-acoustic tomography with limited number of acoustic detectors, *IEEE Trans Image Proc.*, 2000 (to be submitted).
2. A.A. Oraevsky, A.A. Karabutov, V.A. Andreev: Opto-Acoustic Tomography for detection, localization and differentiation of early breast cancer, *Science*, to be submitted.
3. A.A. Oraevsky, V.A. Andreev, A.A. Karabutov, D.R. Fleming, Z. Gatalica, H. Singh, R. O. Esenaliev: Laser optoacoustic imaging of the breast: Detection of cancer angiogenesis, *Proc. SPIE* 1999, **3597**: 352-363.
4. A.A. Oraevsky, A.A. Karabutov, V.A. Andreev, H. Singh, Z. Gatalica, R.D. Fleming: Clinical evaluation of the opto-acoustic imaging for breast cancer, *Radiology*, 2000 (to be submitted)
5. V.A. Andreev, A.A. Karabutov, V.S. Solomatin, E.V. Savateeva, V.A. Aleynikov, Y.V. Julina, D.R. Fleming, A.A. Oraevsky: Optoacoustic Tomography of tumors in the breast, *Proc. SPIE* 2000; 3916: 36-47.
6. A.A. Karabutov, A.A. Oraevsky: Ultimate sensitivity of wide-band detection for laser-induced ultrasonic transients, *Proc. SPIE* 2000; 3916: 228-239.
7. A.A. Oraevsky, "Optoacoustic tomography of deeply embedded tumors and early subsurface lesions", OSA-EPS Conference on Biomedical Optics, Munchen, FRG, June 1999 (INVITED).
8. A.A. Oraevsky, Opto-acoustic imaging of breast cancer", NIH BECON Symposium on Biomedical Imaging, Bethesda, MD, June 1999 (INVITED).
9. A.A. Oraevsky, Opto-acoustic tomography for *in-vivo* detection of cancer", Gordon Conference on Photoacoustic and Photothermal Phenomena, New London, NH, July 1999 (INVITED).
10. A.A. Oraevsky: Visualization of early cancer with opto-acoustic tomography, International Conference on Photoacoustic and Photothermal Phenomena-11, Kyoto, Japan, June 25-29, 2000, pp. 27 (INVITED).

ROBERT W. STROZIER, P.L.L.C.

A FIRM SPECIALIZING IN INTELLECTUAL PROPERTY LAW INCLUDING
PATENT, TRADEMARK, COPYRIGHT, TRADE SECRET LAW,
UNFAIR COMPETITION AND RELATED MATTERS

2925 BRIARPARK, SUITE 930
HOUSTON, TX 77042
TELEPHONE: 713/977-7000
TELECOPIER: 713/977-7011

August 29, 2000

Garold G. Breit, Director
Office of Technology Transfer
The University of Texas Medical Branch
3.118 Administration Annex Building
301 University Blvd.
Galveston, TX 77555-0114

RE: **PCT Ser.No. PCT/US00/; Filed: 8/7/00**
Title: Optoacoustic Monitoring of Blood Oxygenation
UTMB Ref. No.: ; Our Ref. No.: 98006/08PCT

Dear Garold:

Please find enclosed for your records the photocopies of the **PCT Application** for the above-referenced matter.

Under the PCT regulations, the PCT will publish your application 18 months from the filing date of your original United States patent application. At 19 months from the United States filing date, we recommend that you request **Preliminary Examination** of your PCT application requesting the European Patent Office to perform the examination. Preliminary Examination generally costs about $1,000 depending on the current exchange rate. Preliminary Examination extends the time for selecting foreign countries by another 10 month to 30 months for the United States filing date. Preliminary Examination also provides us with valuable information concerning prosecution in Europe and possibly Japan. We will send you additional reminders regarding Preliminary Examination in due course.

If you have any questions or comments, please call me.

Very Truly Yours,

Robert W. Strozier

RWS/sls
Enclosures
cc: Dr. Rinat Esenaliev
Dr. Massoud Motamedi
Dr. Donald Prough
Dr. Alexander Oraevsky

Invited Paper

Opto-acoustic tomography of breast cancer with arc-array-transducer

Valeri G. Andreev, Alexander A. Karabutov, Sergey V. Solomatin, Elena V. Savateeva, Vadim Aleynikov, Yulia V. Zhulina, R. Declan Fleming*, and Alexander A. Oraevsky

Center for Biomedical Engineering, *Department of Surgery
University of Texas Medical Branch, Galveston, TX 77555

ABSTRACT

The second generation of the laser optoacoustic imaging system (LOIS-2) for breast cancer detection, localization and characterization using a 32-element arc-shaped transducer array was developed and tested. Each acoustic transducer was made of 110-μm thick SOLEF® PVDF film with dimensions of 1mm x 12.5 mm. The frequency band of transducer array provided 0.4-mm axial in-depth resolution. Cylindrical shape of this 10-cm long transducer array provided an improved lateral resolution of 1.0 mm. Original and compact design of low noise preamplifiers and wide band amplifiers was employed. The system sensitivity was optimized by choosing limited bandwidth of ultrasonic detection 20-kHz to 2-MHz. Signal processing was significantly improved and optimized resulting in reduced data collection time of 13 sec. The computer code for digital signal processing employed auto-gain control, high-pass filtering and denoising. An automatic recognition of the opto-acoustic signal detected from the irradiated surface was implemented in order to visualize the breast surface and improve the accuracy of tumor localization. Radial back-projection algorithm was used for image reconstruction. Optimal filtering of image was employed to reduce low and high frequency noise. The advantages and limitations of various contrast-enhancing filters applied to the entire image matrix were studied and discussed. Time necessary for image reconstruction was reduced to 32 sec. The system performance was evaluated initially via acquisition of two-dimensional opto-acoustic images of small absorbing spheres in breast-tissue-like phantoms. Clinical ex-vivo studies of mastectomy specimen were also performed and compared with x-ray radiography and ultrasound.

Keywords: *Opto-acoustic imaging, breast cancer, transducer, laser*

1. INTRODUCTION

In previous publications[1-4] we described the basic ideas, principles and the first clinical prototype of the laser optoacoustic imaging system (LOIS-01). This system LOIS–01 was assembled of a compact Nd:YAG laser, fiberoptic light delivery system, a linear array of 12 wide-band acoustic transducers, and a data acquisition card operated by computer. LOIS-01 was successfully tested in imaging mastectomy specimen. Total of fifteen radical mastectomy specimens was investigated at UTMB and UT/MDACC. In all of 15 cases the tumor location was detected and its depth and relative position were measured. Comparison of opto-acoustic images with those of X-ray radiography, MRI and ultrasound imaging performed *in vivo* revealed good correlation in tumor size and location. A pronounced opto-acoustic contrast of 200-450% between breast tumors and normal breast tissues was demonstrated. This contrast substantially exceeds any other endogenous tissue contrast currently utilized in clinical ultrasonography, MRI and X-ray mammography. Based on literature data and our gross observations of tumor cross-sections we hypothesize that the opto-acoustic contrast results primarily from increased optical absorption in the dense microvascularity of the tumors[5].

Correspondence: email: alexander.oraevsky@utmb.edu, http://www2.utmb.edu/cbme/optoacoustic_imaging_&_spec.htm, phone: 1-409-772-8348

In *Biomedical Optoacoustics*, Alexander A. Oraevsky, Editor,
Proceedings of SPIE Vol. 3916 (2000) • 1605-7422/00/$15.00

In patients receiving radiotherapy, tumors were found to contain enhanced concentration of dense highly scattering fibrotic tissue. Especially designed for *in vitro* studies LOIS-01 was characterized by relatively high sensitivity (30 μV/Pa), but was rather cumbrous. A small number of acoustic transducers (12) in receiving linear array limited the lateral resolution of images. The objective of the present study was to fabricate, assemble and test the prototype of laser opto-acoustic imaging system (LOIS-02) for clinical investigations. Design of the new system had to be compact and suitable for performing studies *in vivo*. The resolution of acoustic transducer array had to be improved for small tumor detection and measurement of its dimensions. New signal and image processing employed had to allow operator to reconstruct tumor image in a short time after data collection.

2. MATERIALS AND METHODS

2.1. Arc array transducer

A specially designed array of PVDF acoustic transducers was employed in LOIS-02. The array had 32 rectangular piezoelectric transducers of 1x12.5 mm dimensions and 3.85 mm distance between transducers (see Fig.1). Piezoelectric polymer PVDF of 110-μm thickness was used for transducer fabrication. Low acoustic impedance and ability to operate in wide ultrasonic frequency band are the advantages of PVDF for detection of opto-acoustic profiles. The transducers were located on arc surface of 60-mm radius. This geometry provided a high resolution in the vicinity of focal zone. Backing material was used for mechanical matching of transducer and damping reverberations after detection. When transducer is excited by acoustic pulse it vibrates at its natural resonance frequency.

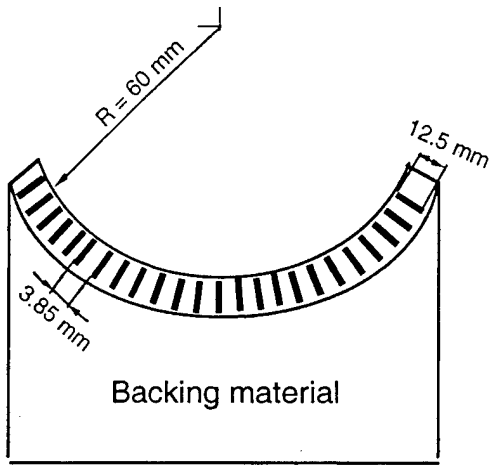

Figure 1. Schematic diagram of arc transducer array.

If acoustic impedance of backing material is similar to that of transducer the ringing could be damped out and the frequency bandwidth increased. The front surface of transducer array was covered by aluminum film to reduce external electric noise. The thickness of Aluminum layer was optimized for the best relation of ultrasound penetration and electric noise reduction. Transducer array housing also was made of aluminum. Acoustic isolating material was placed between piezoelectric elements and housing to prevent ringing of the housing that follows the vibration of the piezoelectric elements themselves.

Absolute sensitivity of each transducer was measured. Results of this calibration are presented in Fig. 2. The mean sensitivity value for transducer array of $S = 6$ μV/Pa is three times lower than the ultimate theoretical value. The ultimate theoretical sensitivity of transducers can be calculated on the basis of piezoelectric properties of PVDF material employed:

$$S = g_{33} d . \qquad (1)$$

where g_{33} is the piezoelectric pressure constant of material, d is the thickness of PVDF film.

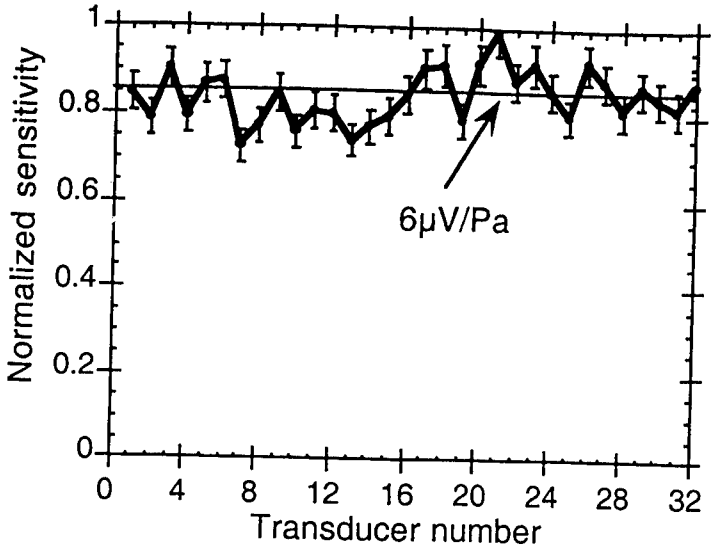

Figure 2. The sensitivity of transducers in the array. Maximum corresponds to the sensitivity of 7 μV/Pa.

Some portion of acoustic energy can be lost due to reflection at the boundary of shielding layer and piezoelectric film. The defects of bonding of these two layers give rise to additional losses. One also has to take into account small value of capacitance of piezoelectric element. The capacitance C_T can be found as:

$$C_T = \frac{\varepsilon\varepsilon_0 A}{d} \tag{2}$$

where A is the surface area of a piezoelement, $\varepsilon\varepsilon_0$ is the dielectric permittivity. In our case the capacity of each transducer was about 10 pF. This value is compared to the stray capacitance of connecting wires and input capacitance of electronic preamplifier. The shunting effect is the source of additional loses of sensitivity in the system. It is difficult to calculate all possible losses of acoustic energy, therefore the direct measurements of transducers sensitivity in array is of great importance. The variability on the sensitivity between array elements is about 15% due to the lack of reproducibility in the manual assembly process.

2.2. Sensitivity of small tumor detection

One of the important parameters of LOIS is the ultimate sensitivity for small tumor detection. Let us consider a tumor as a sphere of radius a with optical absorption coefficient μ_a. The maximum depth of the tumor detection can be evaluated as:

$$z_{\max} = -\frac{1}{\mu_{eff}} \ln\left(\frac{2p_N r}{\Gamma \mu_a a F_0}\right) \tag{3}$$

where μ_{eff} is the effective light attenuation coefficient in breast tissue, r is the distance between the tumor and transducer.

Fluence F_0 of laser pulses at the breast surface must be less then 0.1 J/cm^2 due to safety requirement for medical laser procedures. The parameter Γ characterizes the efficiency of thermo-acoustic excitation in the media. For live biological tissues at 37 °C this parameter varies in the range 0.40 – 0.85 being maximal in fatty tissues. The effective noise pressure p_N is calculated for signal-to-noise ratio (SNR) equal 1. The root-mean-square of noise voltage U_{RMS} was measured

for each transducer. This value is defined by the thermal noise of transducer capacitance and input noise of preamplifiers. For LOIS-2 the measured value of U_{RMS} was about 30 μV. The noise voltage is reduced $\sqrt{N}$ times if the procedure of averaging by N pulses is employed. We used N=16 in our measurements that allowed us to get value of effective noise pressure as 1.3 Pa. Substituting p_N in formula (3) yields the maximum depth of tumor detection of about 6 cm assuming the tumor to be a sphere of 2 mm diameter with μ_a =1 cm^{-1}.

2.3. Lateral resolution

A spatial distribution of acoustic field in the focal surface of array can be described by corresponding expression for the focused arc transducer[3]:

$$p_f = p_{f0}\left|\frac{2J_1(kx\Theta_{\max})}{kx\Theta_{\max}}\right| \tag{4}$$

where p_{f0} is the pressure amplitude in the focal zone, k is the wave number, $\Theta_{\max} = \arcsin(r/R)$ is the angular aperture of array, defined by the radius of arc curvature R and the aperture r (see Fig.4). The size of focal waist δ_l defines the lateral resolution of the array. A value of focal waist can be found from the relation (4) as the distance between zeroes of pressure of −1 and +1 orders:

$$\delta_l = 1.22\frac{\lambda}{\arcsin(r/R)} \tag{5}$$

where λ is the wavelength of ultrasound wave.

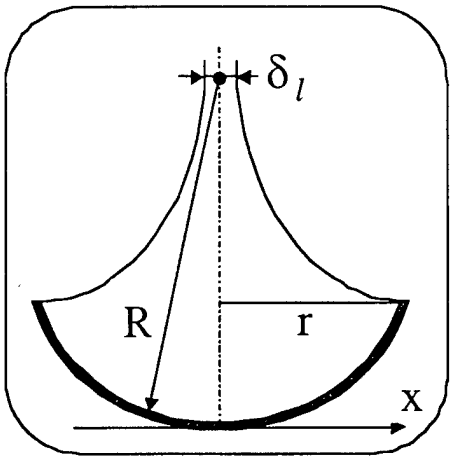

Figure 4. Schematic diagram of directivity of acoustic detection for an arc-shaped transducer.

For our transducer array the ratio r/Requals approximately 0.87, therefore the expression (5) can be simplified, yielding $\delta_l \approx 1.22\lambda$. This estimation is valid for the monofrequency acoustic waves. In case of pulsed detection it is necessary to take into account the frequency spectrum and to choose the value of effective λ correctly. The expression (5) provides correct results when all transducers in array are involved in focused pattern formation. A rectangular transducer with side dimension **b** has directivity pattern with angular width α measured at −3 dB level given by $\alpha = \arcsin(0.45\lambda/b)$ (b=1 mm for the transducer employed in our studies). This means that the lower the ratio of λ/b (or the lower the value of λ with fixed value of b), the narrower the directivity pattern of a single transducer and smaller the space with resolution defined by the value of λ. Therefore the resolution depends on the position of tumor relative to the array. In the vicinity of the focal zone (i.e. for the points of location inside the circle of 1-cm radius with center in the

geometrical focus of the array) the resolution is less 1-mm. In the main part of space the resolution is about 1mm< δ_l <2 mm.

2.4. Axial in depth resolution

The axial (in-depth) resolution of the pulsed opto-acoustic system operating under irradiation conditions of temporal pressure confinement is directly defined by the detection bandwidth of acoustic transducers. Two coherently emitting spherical acoustic sources with radius a will be detected as separate objects if the space between their centers equals or greater than $\Delta z = 2a$. For correct detection of pulsed opto-acoustic waveform excited in absorbing sphere of radius a, it is necessary to detect opto-acoustic signals within a wide ultrasound frequency band of 0 - f_b,:

$$f_b = 0.75 c_s / a \tag{6}$$

where c_s is the speed of sound, f_b, is the upper limit of the ultrasonic frequency band in the frequency spectrum of N-shaped signal emitted by the small sphere.

Therefore the following inequality must be satisfied: $f_b < f_{\max}$, where f_{max} is the upper frequency limit of ultrasound detector. Using expression (6) for f_b, one can obtain:

$$\Delta z > 1.5 \frac{c_s}{f_{\max}} \tag{7}$$

The upper frequency limit of ultrasonic detection band f_{max} is defined by the transducer thickness and the frequency bandwidth of preamplifier employed. In our design the upper frequency limit was 6 MHz, that provided 0.38 mm axial in-depth resolution.

2.5. LOIS-02 Description

Schematic diagram of LOIS-02 is shown in Fig. 5. A Nd:YAG laser (Big Sky Lasers, MA) operating at the wavelength of 1064 nm was used as a source of near-infrared pulses of 10-ns duration. A quartz optical fiber was employed for the laser pulse delivery to the tissue surface. The fiber-optic system was attached to a three-dimensional translation stage driven by a step motor. An electronic data acquisition system was synchronized with the linear translation along the chosen direction.

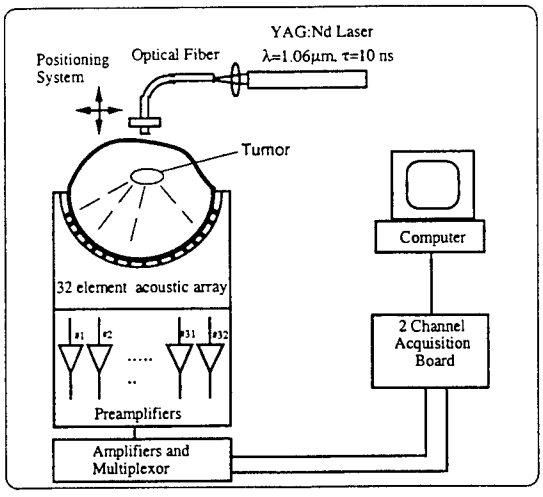

Figure 5. Schematic diagram of LOIS-02.

Breast phantoms and mastectomy specimens were placed on the surface of the acoustic array with m=32 elements. Transducer array housing was fixed vertically in a specially designed holder, which provided a convenient access to the samples. A circuit board with 32 identical preamplifiers was placed in the same housing in the vicinity of transducers. Each preamplifier had a 1 MOhm electrical input impedance and low output impedance of 50 Ohm. It allows one to match the

output impedance of piezoelectric elements and the connecting cable in order to improve the sensitivity and the signal-to-noise ratio. The voltage of electrical signals from preamplifiers was amplified, and signals were then digitized with a PDA-12 data acquisition card with two input channels (SignaTech, CA). A multiplexor sequentially connected thirty-two amplifier outputs with the two input channels of the data-card. Acquired data were stored in a computer for further processing.

2.6. Data processing in LOIS-02.

Signal processing algorithm realized in LOIS-02 is shown schematically in Fig.6. Each signal detected by acoustic transducers in the array consists of the following three components: (1) a sharp peak produced at the very surface of the medium under investigation, (2) a low-frequency smooth-rise exponential slope produced by the attenuation of light intensity inside tissue, and (3) short N-shaped pulses generated by small absorbing tumors. We assumed here that the tumor is a sphere of radius a. The duration of the N-shaped pulse is defined by the time of sound propagation through the sphere diameter. The delay in time of signal arrival depends on tumor location relative to transducer. Therefore position of the tumor and its dimensions can be determined from the opto-acoustic signal.

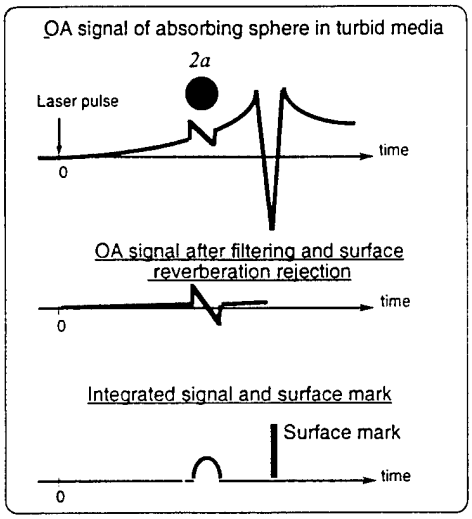

Figure 6.

Before the signal could be used for image reconstruction, it is necessary to eliminate completely its low frequency component associated with homogeneous light attenuation inside the tissue, because it can significantly decrease the image contrast. This was achieved in LOIS with high-pass numeric filtering with RC cells. The value of RC~10 μs defines the cut-off ultrasonic frequency, and the sharpness of the filter cut-off is defined by the number of RC cells. The greater the number of elementary RC cells, the steeper the slope of the filter transfer function. The cut-off frequency and the slope of the transfer function of the filter could be varied conveniently by the imaging operator.

The signal generated by laser pulses in the subsurface layer (very close to the surface) possesses maximum amplitude over the entire detected course. Therefore, the signal gradient is maximal at the tissue surface, which yields high ultrasound frequencies. High ultrasound frequencies that fall near the resonance frequency, f_{max}, of piezo-elements can induce significant reverberation in the transducer. Our transducers were designed to damp resonance frequencies and widen the range of detectable frequencies. Nevertheless, a strong reverberation takes place after the arrival of the signal from the surface of tissue. These reverberations do not affect the useful part of the opto-acoustic profile. Besides, it is convenient to employ the sharp peak with high gradient (derivative) for automatic determination of the tissue surface. The position of absolute minimum in the signal was considered as the position of the irradiated tissue surface. The controlling computer generated numerical signal at the surface position determined for each transducer and stored these data in a separate file. All data samples were cut off the signal after arrival of the signal generated at the tissue surface. Integrated signals were used as input data for the image reconstruction code. The surface-marks generated by computer were used for the surface

visualization. Combined image contained the surface and the tumors, provided information about tumor location relative to the irradiated surface.

2.7. Image reconstruction algorithm

Let us consider the case of thermo-optical excitation of acoustic waves in homogeneous medium with coefficient of optical absorption μ_a. The temporal integral of acoustic pressure detected by transducer located in the point $\mathbf{r}$ can be expressed in the following form[6]:

$$u(\vec{r},t) = \int_{-\infty}^{t} p(\vec{r},t')dt' = \frac{\beta}{4\pi C_p}\int_V \frac{\mu_a(\vec{r}')I(\vec{r}')L(t-\frac{|\vec{r}-\vec{r}'|}{c_s})}{|\vec{r}-\vec{r}'|}d\vec{r}'. \quad (8)$$

where β is the thermal coefficient of volume expansion, C_p is the specific thermal capacity of the medium, L is the laser waveform function. All other notations used in formula (8) are shown in Fig.7.

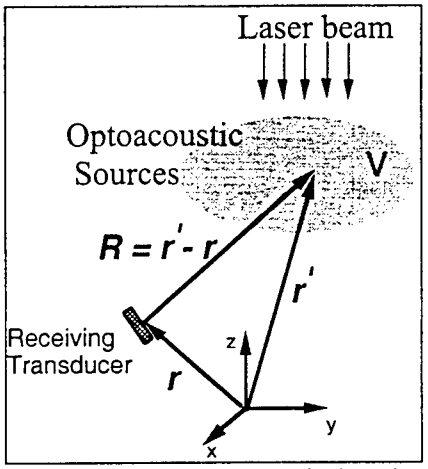

Figure 7. Geometry of the opto-acoustic detection.

Integral is calculated over the entire space. It means that the acoustic pressure $p(\vec{r},t)$ at the time moment t and in the point $\mathbf{r}$ is determined by the thermal sources located in the spherical layered volume with radius $|\vec{r}-\vec{r}'|$ and thickness $d\vec{r}'$. Acoustic waves arrive to the measurement point $\vec{r}$ with time delay $|\vec{r}-\vec{r}'|/c_s$. If the laser pulses are sufficiently short, then generation of thermal sources may be considered instantaneous and the laser waveform function can be expressed in the form: $L(t) = \tau_L\delta(t)$, where τ_L is the laser pulse duration, $\delta(t)$ is the delta function. Equation (8) for short laser pulses can be written in the following form:

$$u(\vec{r},t) = \frac{\beta}{4\pi C_p}\int_V \frac{\mu_a(\vec{r}')F(\vec{r}')\delta(t-\frac{|\vec{r}-\vec{r}'|}{c_s})}{|\vec{r}-\vec{r}'|}d\vec{r}' \quad (9)$$

where F is the laser fluence. Let the surface Σ be the spherical surface of radius R with origin at the position of receiving transducer. Radius of the sphere is defined by the time of sound propagation from the surface to the transducer. Vector $\vec{R}$ can be presented as $\vec{R} = c_s t\vec{n}$, where $\vec{n}$ is the unit vector of the surface element $d\Sigma$. Thus, the temporal integral of acoustic pressure can be expressed as:

$$u(\vec{r},t) = \frac{\beta}{4\pi C_p c_s t}\int_\Sigma Q(\vec{r}+c_s t\vec{n})d\Sigma, \quad (10)$$

where function $Q(r) = \mu_a(r)F(r)$ describes the spatial distribution of thermo-acoustic sources.

Equation (10) can be considered as the fundamental equation for the opto-acoustic tomography. The temporal integral of pressure profile detected by transducer at the time t is the superposition of thermal sources located on the sphere of radius $R = c_s t$. The product of light absorption coefficient and light fluence at this spherical surface determines acoustic amplitude of the thermal source.

2.8. Image processing

An image reconstruction algorithm based on Radon transform with limited set of data was proposed for the opto-acoustic tomography[7]. However, this method does not yield satisfactory resolution even with significant number of transducers employed. We adopted a radial back-projection algorithm, earlier developed for the ultrasound imaging[8]. For the reconstruction of two-dimensional opto-acoustic images we used signal integrals shown in Fig 6 and projected them back onto the two-dimensional grid taking into account the directivity pattern (angle of acceptance) of each transducer. The entire image field resulted from radial back-projection algorithm can be written in the following form:

$$\xi(\vec{r}) = \sum_{n=1}^{m} u_n(|\vec{r} - \vec{r}_n|/c_s)\,|\vec{r} - \vec{r}_n| \tag{11}$$

where u_n is the integrated signal of the n-th transducer, $\vec{r}_n$ is the radius vector of the n-th transducer, m is the number of transducers in array. The image represents distribution of a product of thermo-acoustic efficiency, optical absorption and absorbed laser energy. The back-projected images are noisy and their contrast is insufficient for correct object recognition. Therefore an image filtration procedure was employed:

$$\xi_2(\vec{r}) = \frac{1}{4\pi^2}\int F_\xi(\vec{\omega})H(\vec{\omega})\,e^{i\vec{\omega}\vec{r}}\,d\vec{\omega} \tag{12}$$

where $F_\xi(\vec{\omega}) = \int \xi(\vec{r})e^{-i\vec{\omega}\vec{r}}\,d\vec{\omega}$ is the 2D Fourir spectrum of the back-projected image, $H(\vec{\omega}) = |\vec{\omega}|e^{-(|\vec{\omega}|/\sigma)^2}$ is the filter transfer function, $\vec{\omega} = \{\omega_x, \omega_y\}$ is the vector of spatial frequencies. The parameter σ allows us to modify the filter bandwidth and the steepness of filter characteristic. It can be done manually by operator or automatically. In automatic procedure the parameter σ was chosen if additional condition for image quality was applied. The filter parameter σ was optimized employing the criterion of maximum contrast of the resulting image.

2.9. Time parameters of LOIS-02.

Data acquisition time in LOIS-02 equals 13 sec for one fiber position. The laser pulse repetition rate is assumed to be 20 Hz and 16 pulses for averaged acquisitions are employed. Four seconds is needed for data processing and back-projected image formation. Image filtration and its optimal processing takes 10 sec. Total time equals 32 sec.

3. RESULTS AND DISCUSSION

3.1. Spheres in milk

Laser optoacoustic imaging system was tested in various phantoms. Two-dimensional image of a sphere 8-mm in diameter in milk is shown in Figure 8. Whole milk was diluted by water to obtain the effective optical attenuation coefficient 1.2 cm^{-1} to mimic the optical properties of the breast tissue. Optical absorption coefficient of the sphere was about 1.0 cm^{-1}. This value is typical for the light absorption in tumors we measured in mastectomy specimen[4]. The sphere was located near the focal zone of transducer array. Axes in images are scaled in millimeters. Position of the transducer array is marked by arc dotted line. Surface position was detected and reconstructed by using the computer-generated surface marks. In this particular case the surface was flat, therefore it was marked by a straight line. A real surface position (72-mm) was in agreement with automatically detected value. The center sphere depth (19-mm) in image corresponded very well with measured value.

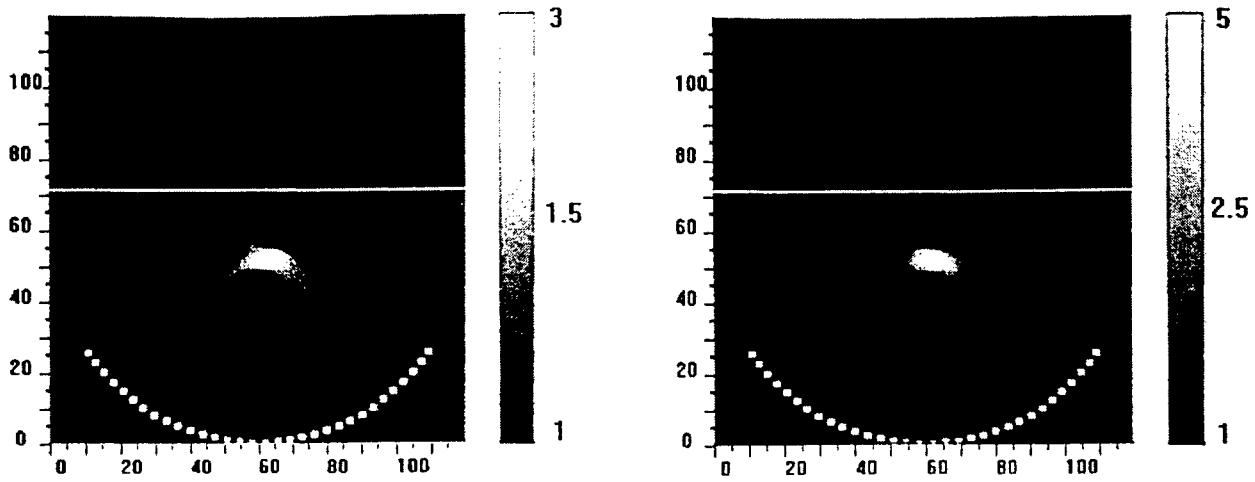

Figure 8. Opto-acoustic image of absorbing sphere in milk. Axes are scaled in millimeters.

Back-projected image presented on the left side of Figure 8 is noisy. Filtered image shown on the right side of the Fig. 8 demonstrates the noise reduction. The contrast of filtered image (right) was increased 1.7 times compared with unfiltered image (left). The image of sphere differs from the correct spherical shape. This fact has a simple explanation. As the angle of acceptance of sphere by the transducer array was about 120° only one-third of data needed for complete image reconstruction were collected and employed in image reconstruction.

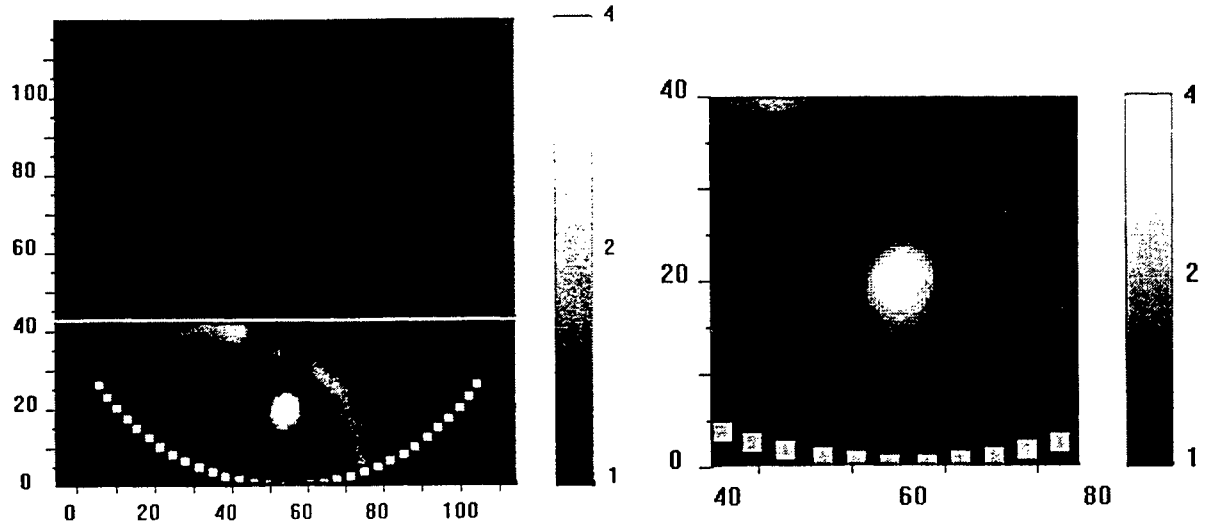

Figure 9. Sphere of 8-mm diameter in milk in near array zone. Milk surface is marked by a straight line.

An increase of the acceptance angle for the spherical object resulted in a better reproduction of its shape in image, as clearly depicted in Fig. 9 showing an image of a sphere in the near zone. The angle of acceptance in this case is about 200° and as a consequence the shape of image highly correlates with real shape of the sphere. Fig. 9 (right) presents the twice-magnified fragment of the sphere image. An arc-shaped artifact could be seen in Fig. 9 and resulted from the opto-acoustic signal generated at the milk surface. This surface signal was not filtered completely for only two of 32 transducers, but it was enough to yield such an artifact. Fig. 9 demonstrates the importance of optimal signal filtering for rejection of artifacts. The filtration procedure demonstrated in Fig.8 could yield complete elimination of all artifacts due to surface signals.

3.2. Spheres in gelatin phantom

A gelatin phantom with two absorbing spheres was made. A cylindrical shape of the phantom with 120-mm diameter provided a perfect acoustics contact with transducer array. The effective light attenuation coefficient of 1.2 cm^{-1} was similar to typical value for normal breast tissue *in vivo* at the wavelength of 1064 nm. A tumor phantom was made of the same gel and colored with the bovine hemoglobin. The "tumors" had spherical shape and absorption coefficient of 1.0 cm^{-1}. Diameter of the spheres was approximately 8 mm. The relative position of spheres in the phantom is shown schematically in Fig.10 (right diagram). The depths of spheres were 27 and 34 mm respectively, and the distance between their centers was about 11 mm. The procedure of measurements was as follows.

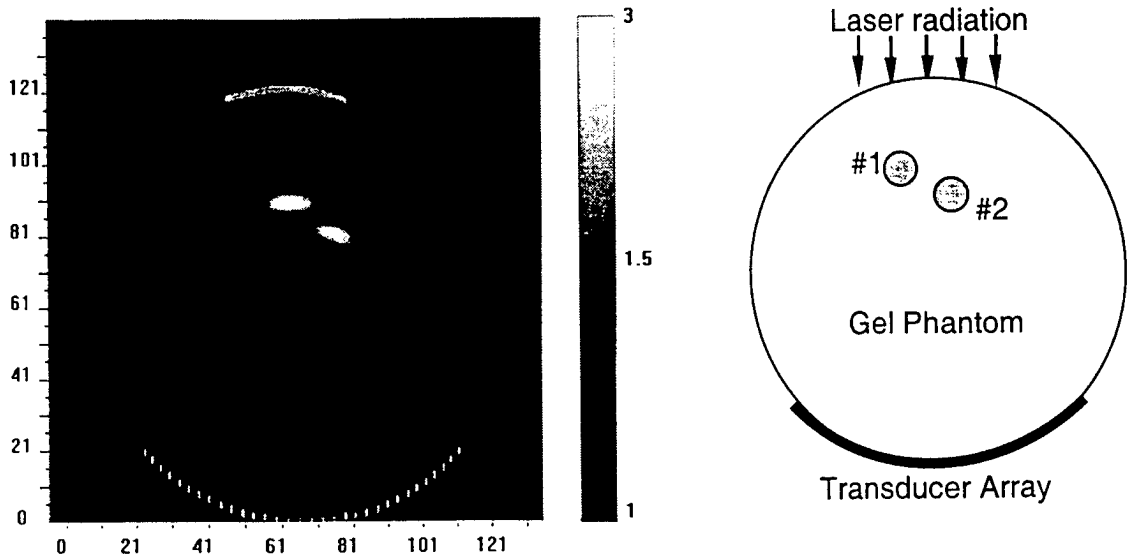

Figure 10. Image of two spheres in gel phantom.

The gelatin phantom was placed on the transducer array surface for the opto-acoustic scanning. Absorbing spheres were located above the transducer array beyond its focal zone. The transducer array surface was preliminary moistened in order to provide good acoustic coupling between phantom and the transducer. Optical fiber was installed at the 10-mm height from the phantom surface. The fiber was moved along the acoustic array axis with 6-mm intervals. The length of the opto-acoustic scan of 30-mm was sufficient to achieve clear resolution of images of each sphere. Full set of 32 acoustic signals was obtained at each fiber position. As a result, complete table of data corresponding to one scan was acquired.

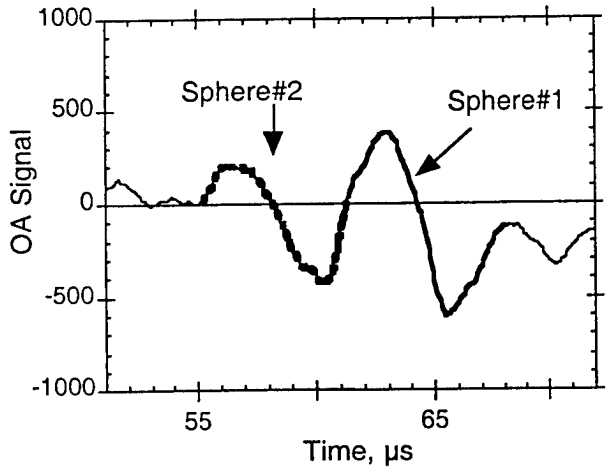

Figure 11. OA signal of two absorbing sphere in phantom detected by one of the central transducer in array.

An image of two spheres is presented in Fig.10 (left). Procedure of image filtering was employed to provide the best contrast of the image (~300%). Two spheres are clearly resolved and depicted as two separate objects. The relative position of spheres and their depths are in good agreement with their real location. A part of the arc phantom surface in the poits of surface illuminations is also presented in Fig.10. The image of the surface was reconstructed separately using the surface marks and then it was superimposed on the sphere image. Partial profile of a signal detected by one of the central transducers in array is presented in Fig.11. Two N-shaped signals that were excited in spheres can be clearly seen. Amplitude of the signal in sphere located close to the phantom surface (sphere #1) is higher then in sphere #2. Therefore, the brigthness and the image contrast is higher for the sphere #1.

3.3. Breast mastectomy specimen

Breast specimens were obtained after radical mastectomy and examined within the first ten minutes after surgical excision. It provided specimens that underwent minimal alterations of tissue optical properties, except some blood was drained form the specimens. The mastectomy specimens were measured to determine tumor geometry. Location of tumors was not known prior to opto-acoustic imaging procedure. However, tumors were sometimes palpable and biopsy incision was visible on the spared segment of skin. Opto-acoustic image of breast with carcinoma is presented in Fig.12.

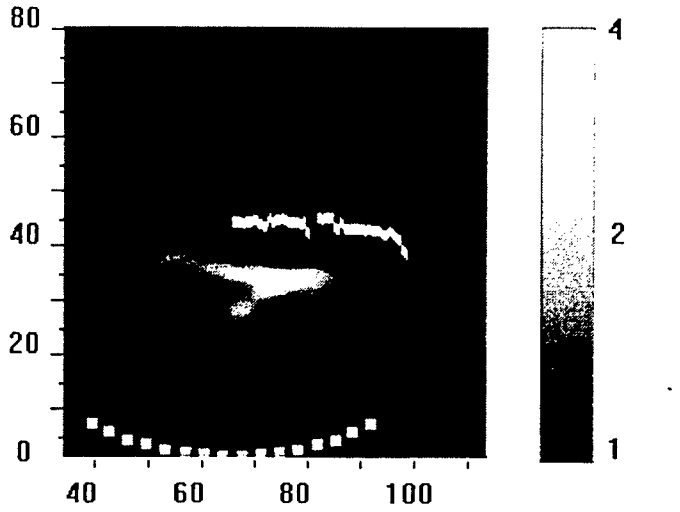

Figure 12. Opto-acoustic image of a malignant tumor. UTMB Patient # 408112P.

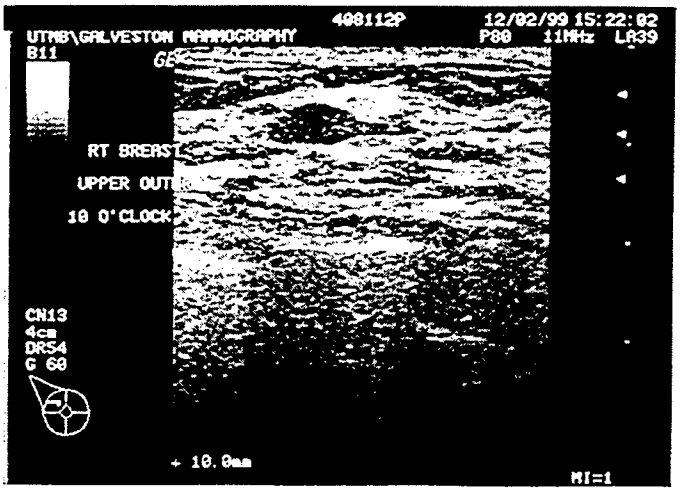

Figure 13. Ultrasound image of tumor UTMB Patient # 408112P.

Fifteen fiber positions with 4-mm interval were employed for data collection and subsequent image reconstruction. The scan passed directly over the tumor. The tumor core, horizontal tail and a small sprouts may be clearly seen in the opto-acoustic image (confirmed by subsequent pathology examination). The dimension of a tumor core can be estimated as 10x7 mm. Tumor was detected at the depth of 11 mm from the surface. Skin was removed from most part of the specimen, therefore the irradiated surface is depicted as a rough line. Contrast between the tumor and surrounding normal tissues in this image exceeds 350%.

The ultrasound image of the same tumor, however measured in *vivo* is presented in Fig. 13. The core of tumor and its long tail may also be seen in this image. However, small sprouts are not visible to limited acoustic contrast.

4. CONCLUSION

The second generation of the laser optoacoustic imaging system LOIS-02 for breast cancer detection with 32-element transducer array was developed and tested in phantoms and mastectomy specimens. Sensitivity of LOIS-02 permits detection of 2-mm tumors at the depth of 6 cm. In depth resolution equals 0.4 mm, lateral resolution is 1-2 mm depending on position of tumor relative to the transducer array.

LOIS-02 is the basis for a new system, which will be used for *in vivo* studies. In vivo optoacoustic imaging protocol is currently approved at UTMB. Two *in vivo* systems are being fabricated: compact 2D real-time system and 3D high-resolution system with 60-sec data acquisition time.

ACKNOWLEDGMENTS

This work was supported by the National Cancer Institute (grant #R29-CA80221) and DOD Breast Cancer Research Program, US Army (grant #DAMD17-99-1-9404).

REFERENCES

1. A.A. Oraevsky, S.L. Jacques, R.O. Esenaliev, F.K. Tittel: Time-Resolved Optoacoustic Imaging in Layered Biological Tissues", In: "Advances in Optical Imaging and Photon Migration", vol. 21, ed. by R.R. Alfano, Academic Press (1994) pp. 161-165.
2. A.A. Oraevsky, R.O. Esenaliev, S.L. Jacques, F.K. Tittel: Laser Opto-Acoustic Tomography for medical diagnostics: principles, *Proc. SPIE* 1996; **2676**: 22-31.
3. A.A. Oraevsky, V.G. Andreev, A.A. Karabutov, R.O. Esenaliev: Two-dimensional optoacoustic tomography: array transducers and image reconstruction algorithm, *Proc. SPIE* **3601**: 256-267 (1999).
4. A.A. Oraevsky, A.A. Karabutov, V.G. Andreev, R.O. Esenaliev: Laser opto-acoustic imaging of the breast: Detection of cancer angiogenesis, *Proc. SPIE* **3597**: 352-363 (1999).
5. N. Weidner, J.P. Semple, W.R. Welch, and J. Folkman: Tumor angiogenesis and metastasis - correlation in invasive breast carcinoma, *New Engl. J. of Med.*, 324, pp. 1-7, 1991.
6. G.S. Kino: "Acoustic waves. Devices, imaging, and analog signal processing", Prentice-Hall, Englewood Cliffs, 1987.
7. P. Liu: Image reconstruction from photoacoustic pressure signals. *Proc. SPIE* **2681**: 285 – 296 (1999).
8. K.C. Ternovoy, M.V. Sinkov: "Introduction to modern tomography", Naukova Dumka, Kyiv, Ukraine (1996).

Laser Opto-Acoustic Imaging of the Breast: Detection of Cancer Angiogenesis

Alexander A. Oraevsky[1], Valeri A. Andreev[1], Alexander A. Karabutov[1], Declan R. Fleming[2], Zoran Gatalica[3], Harbans Singh[4], and Rinat O. Esenaliev[1]

[1]Biomedical Engineering Center, University of Texas Medical Branch, Galveston, TX 77555
[2]Department of Surgery, [3]Department of Pathology, [4]Department of Radiology,
University of Texas Medical Branch, Galveston TX 77555

ABSTRACT

First clinical prototype laser optoacoustic imaging system (LOIS) for breast cancer detection was designed and fabricated using a compact Nd:YAG laser, fiberoptic light delivery system, a linear array of 12 wide-band acoustic transducers, and a data acquisition card operated by computer with original signal processing and image reconstruction code. Initially images of small absorbing spheres were recorded in the milk with optical properties resembling those of the breast at the wavelength of 1064-nm. The system was optimized for contrast, sensitivity and axial (in-depth) resolution. The small number of acoustic transducers (12), which in turn was determined by the system cost and the time of image acquisition limited the lateral resolution of the images. Clinical ex-vivo studies on radical mastectomy specimens were performed and compared with x-ray radiography, MRI and ultrasound imaging. The results of our pilot clinical studies showed pronounced opto-acoustic contrast of ~300% between breast tumors and normal breast tissues. This contrast substantially exceeds any other endogenous tissue contrast currently utilized in clinical ultrasonography, MRI and x-ray mammography. Based on literature data and our gross observations of tumor cross-sections we hypothesize that the opto-acoustic contrast results primarily from increased optical absorption in the dense microvascularity of the tumors. In patients receiving radiotherapy, tumors were found to contain enhances concentration of dense highly scattering fiberotic tissue.

1. INTRODUCTION

Breast cancer has the highest incidence (30%) of all female cancer cases in the USA. About 10% of American women develop breast cancer during their lifetime. It is estimated that 175,000 new cases will be diagnosed and 43,300 deaths will occur as a result of breast cancer this year [1]. Because of the high incidence, even small improvements in breast cancer diagnosis and treatment may save tens of thousand lives every year. Statistics indicates that detection and follow-up in the early stages of cancer offer a much greater chance of survival than detection and follow-up at later stages. This is particularly true for breast cancer.

The gold standard, X-ray radiography (mammography), magnetic resonance imaging (MRI), and ultrasound are the three imaging techniques that are currently available for breast cancer detection. All these techniques have certain advantages for detection and localization of a specific tissue abnormality. However, all of them are not free of limitations when applied for the breast cancer imaging. The major limitation of X-ray mammography is its incapability to detect lesions in radiologically dense breast. The minimal size of tumors detectable by mammography is about 5-10 mm if a tumor contains no calcification [2]. X-ray mammography utilizes harmful ionizing radiation.

The main limitation of the ultrasound imaging is a low contrast [3]. On one hand, the detection of tumors in many cases is difficult due to the low contrast in acoustic properties between the tumors and normal tissues.

Part of the SPIE Conference on Optical Tomography and Spectroscopy of Tissue III
San Jose, California • January 1999 SPIE Vol. 3597 • 0277-786X/99/$10.00

On the other hand, heterogeneous structure of the breast yields complex ultrasound images with numerous artifacts resulting from multiple reflections of the ultrasonic waves from tissue boundaries. The minimal tumor size of detection by current ultrasonic imaging systems at a depth of 5-6 cm inside biological tissues is limited to about 10 mm.

The major merit of MRI is high-resolution [4]. This technique is capable of characterizing the tissue hydrogen content and water environment. However, the sensitivity of MRI in many instances is not very impressive, and this technology is also very expensive [4]. The gadolinium contrast agent is used in MRI in combination with dynamic perfusion imaging to visualize tissue vascularity, which helps tremendously to improve cancer detectability [5, 6].

Various types of optical tomography have been proposed for cancer diagnostics and intensively developed during the last decade. Optical tomography is based on differences in optical properties between tumor and normal tissues. The major difference in absorption coefficient results from higher blood content in tumors compared with normal tissues [7] which in turn is associated with increased vascularization (angiogenesis) in rapidly growing tumors [8, 9]. Since hemoglobin of blood is the major chromophore in biological tissues in the visible and near infrared spectral range [10, 11] malignant tumors have higher absorption coefficient than normal tissues. Recent clinical studies that employed optical imaging techniques demonstrated existence of optical contrast of 200-300% between normal and cancerous tissues in the breast [12, 13]. However, strong light scattering and attenuation in biological tissues substantially limit resolution and depth of monitoring for optical tomography.

Several years ago a pulsed laser optoacoustic tomography, combining advantages of optical contrast and sensitive, high-resolution ultrasonic detection was proposed for breast cancer imaging [14-17]. The optoacoustic tomography in forward mode (OAT-F) utilizes acoustic signals induced by laser pulses in tumors and transmitted forward along the axis of laser irradiation to the acoustic transducer [18-20]. Application of a wide-band acoustic detection instead of detection of photons in OAT-F helps to overcome two problems associated with strong light scattering in biological tissues and improve depth of monitoring [20] and spatial resolution [21, 22]. The profiles of acoustic waves generated under irradiation conditions of temporal pressure confinement in the volume of tumors resemble the profile of absorbed laser energy [23]. Tumors with dimensions of 1-10-mm irradiated with laser pulses represent themselves as sources of acoustic waves with ultrasonic frequencies of ~1 MHz to ~100 kHz. Such ultrasonic waves can propagate in biological tissues with insignificant attenuation [24-26]. However, acoustic diffraction in the ultrasonic frequency range $\leq$ 1 MHz is pronounced and must be compensated by integrating the measured signal over the entire time-course of detected signal [27, 28].

The objectives of the present study were: (1) to construct, assemble and test in vitro the first clinical prototype system for breast imaging, (2) to demonstrate detection and localization of breast tumors in mastectomy specimens previously visualized *in vivo* with conventional imaging modalities, (3) to compare contrast between tumors and normal tissues for four techniques (OAT, X-ray mammography, MRI and ultrasound imaging).

2. MATERIALS AND METHODS

2.1. Linear array transducer

A specially designed linear array of PVDF acoustic transducers fabricated by LaserSonix Technologies, Inc. Houston, Texas, was employed in clinical experiments. A photograph of the transducer array is shown in Figure 1. The array had twelve rectangular piezo-elements of 12.5x4.3 in dimensions and 1-mm distance between elements. The ultrasonic frequency band determined by the resonance frequency of element was 50 kHz to 3 MHz at the 1/e level of maximal sensitivity of 30 μV/Pa. The axial (in-depth) resolution of images obtained with the opto-acoustic tomography was 1-mm as determined by the ultrasound band of transducer detection [29]. The lateral resolution of the acoustic transducer array was defined by the total length of the array and the dimensions

of each individual transducer [29]. It was also dependent on the distance between the tumor and the transducer. An average lateral resolution in our clinical experiments was approximately equal 2a, where a is the tumor radius.

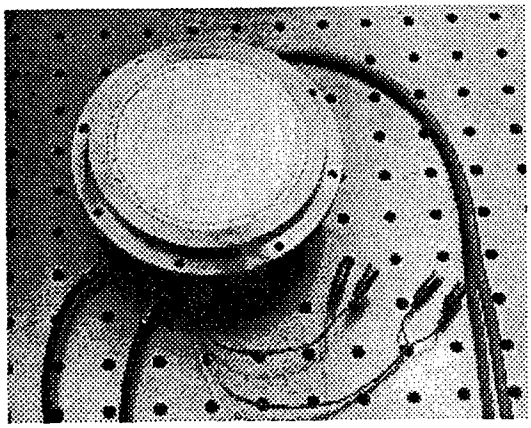

Figure. 1. Photograph of the linear array of 12 transducers housed with 12 charge preamplifiers.

When soft tissue with light absorbing tumors is irradiated with a 10-nanosecond laser pulse, it is heated faster than any thermoelastic expansion may occur. Spherical acoustic waves that propagate from the laser-heated tumors have bipolar N-shaped profiles. The duration of acoustic profiles excited in a spherical absorber of radius a_0 equals $\tau = 2a_0 / c_s$, where c_s is the speed of sound. The smaller the tumor size, the shorter the duration of the acoustic N-pulse. Wide band ultrasonic frequency detection is required for the precise transduction of the acoustic profiles into electric pulses. A two-dimensional image reconstruction algorithm employs electric pulses recorded by an electronic signal acquisition board as input data.

2.2. Two Dimensional Opto-Acoustic Imaging System

A schematic diagram of the first clinical prototype LOIS is shown in Fig. 2. An Nd:YAG laser operating at the wavelength of 1064 nm was used as a source of near-infra-red pulses of 10-ns in duration. An optical fiber was used for the laser pulse delivery to the tissue surface. The fiber-optic system was attached to a three-dimensional positioning stage driven by a step motor. An electronic data acquisition system was synchronized with the linear translation along the chosen direction. Tissue samples were placed on the surface of a 50-mm thick acoustic buffer filled by degassed water. The buffer thickness was sufficient to bring the rear tissue surface in the far detection zone. Thereby all twelve transducers were involved in the opto-acoustic detection, which provided a better lateral resolution. Amplified electrical signals from acoustic transducers were digitized by a PDA-12 data acquisition card with two input channels (SignaTech, CA). A multiplexor sequentially connected twelve amplifier outputs with the two input channels of the data card. A photodiode detecting laser pulses leaking from the rear mirror was applied for synchronization of the optical and acoustic systems. Acquired data were stored in a computer memory for further processing. The data processing procedure and the image reconstruction algorithm were described in our technical publication [29].

LOIS sensitivity is a function of the system detection parameters and tissue properties. The smallest size of detectable absorbing tumor located at a certain depth within the tissue or the largest depth of detection for a tumor particle with certain dimensions can characterize the sensitivity of the opto-acoustic imaging system. The light absorption coefficient for breast tumors depends on the tumor blood content, which may vary in a wide range around μ_a=0.75 cm^{-1} at the wavelength of 1064-nm. The minimum detectable pressure amplitude is limited by the thermoelectric noise of the piezoelement. In our acoustic transducers the effective noise pressure may be estimated at ≈0.5 Pa.

In order to increase the signal-to-noise ratio, an increase in the incident laser fluence may be used. However, in clinical applications the incident laser fluence is limited by a safe level of 0.1 J/cm^2 permitted by the American

national laser safety standards [30]. Earlier, we demonstrated experimentally that a small sphere with low blood content (μ_a=0.5 cm^{-1}) and 1-mm radius can be detected at the depth of 60 mm when a safe level of pulsed laser irradiation is employed [19].

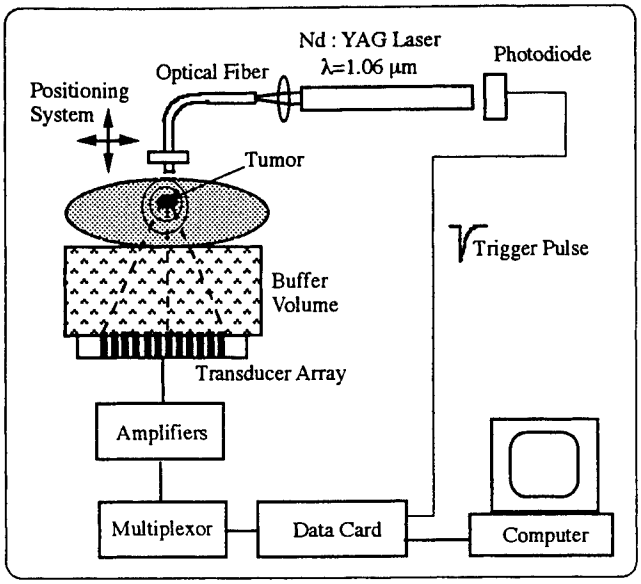

Figure 2. Schematic diagram of LOIS.

In the clinic, the breast samples were examined as fast as possible to avoid irreversible chemical transformations in excised tissue. The factor of time is critical for the use of the genetic biochemical assay in pathology studies. The system was designed to perform opto-acoustic imaging procedure in less than 10 minutes.

2.3. Conventional imaging modalities

X-ray images of the breast phantoms were obtained with the use of clinical mammography machine (Lorad M IV, Lorad Corp., Danbury, CT). The best contrast of x-ray images was achieved with application of molybdenum anode and molybdenum filter at the voltage of 30 kV. Ultrasonography was performed with a modern sophisticated ultrasound machine Sonoline Elegra (Siemens, New York, NY) with various contrast enhancement features. MRI mammography system with 0.5 Tesla magnet (Caprius Corp., Wilmington, MA) employed dynamic perfusion imaging with gadodiomide contrast agent (Omniscan, Nycomed-Amersham, Wayne, PA).

2.4. Phantoms

Breast phantoms were made of 10%-gelatin and had dimensions of 100 x 97 x 57 mm. Water absorption (μ_a = 0.15 cm^{-1} at 1064 nm [20]) provided the absorption coefficient of 0.13 cm^{-1} in the gel phantoms. The typical effective attenuation coefficient, μ_{eff}, for normal breast tissue *in vivo* is about 1.0 to 1.2 cm^{-1} at the wavelength of 1064 nm, while the optical attenuation of the skin is 1.3-1.4 cm^{-1}. Polystyrene spheres were used, to provide effective scattering coefficient of 4 cm^{-1}. Absorption by water and scattering by polystyrene microspheres yielded an effective attenuation of 1.3 cm^{-1} for our phantom.

A tumor phantom was made of the same optically turbid gel and colored with the bovine hemoglobin. The "tumor" had spherical shape and absorption coefficient of 0.75 cm^{-1}. Diameter of the sphere was approximately 8 mm. The sphere was placed on a thin nylon white thread in order to provide its fixed position

inside the gel phantom. Liquid gel at the temperatures very close to the solidification temperature was poured inside a Plexiglas cube. After solidification in a refrigerator the phantom was taken out from the Plexiglas cube and examined with LOIS. The breast phantoms were made acoustically homogeneous and radiologically dense, while the ratio of absorption coefficients of the spheres and surrounding gel was equal 6, a value anticipated between breast tissues and advanced tumors *in vivo*.

2.5. Mastectomy specimen and the imaging procedure

Breast samples were obtained after radical mastectomy and examined within first ten to twenty minutes after excision. It provided us with specimen that underwent minimal alterations of tissue optical properties, except the blood was noticeably drained form the specimen. The mastectomy specimens were measured to determine their dimensions. Location of tumors was not known prior to opto-acoustic imaging procedure. However, often tumors were palpable and a biopsy incision was visible on the spared segment of the skin.

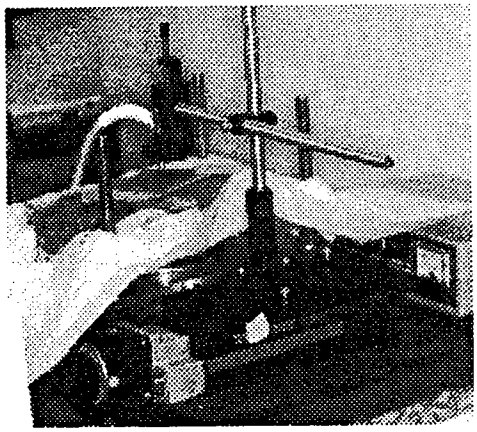

Figure 3. Photograph of mastectomy specimen placed on the transducer array for imaging with LOIS.

Breast samples were placed on the transducer buffer surface for the optoacoustic scanning. The buffer surface was preliminary wetted to provide a good acoustic contact between breast tissues and the transducer. Optical fiber was installed at the 3-mm height from the sample surface. The fiber was moved along the acoustic array axis with 6-mm intervals. The laser beam diameter on tissue surface was about 8-mm. The repetition rate was 10 Hz and the pulsed energy was approximately 48 mJ. The length of the opto-acoustic scan of 72-mm was equal to the length of the acoustic transducer array. At each fiber position a set of acoustic signals were obtained. As a result the complete table of data corresponded to one scan was acquired. Imaging procedure (data acquisition) was performed in vertical direction (along the body axis) two-three times within portions of the breast suspicious to have a tumor.

Gross photographs of the specimens were taken before and during pathological examination. The first stage of the pathological examination (performed immediately after the opto-acoustic tomography) included sectioning of the breast specimen in vertical direction producing 0.5-cm to 1-cm thick slices. Opto-acoustic images were reconstructed based on the measured pressure profiles. The images were compared with x-ray mammograms, ultrasonograms and MRI images, when available, and with gross and histological pathology findings obtained during routine pathologic examination.

3. RESULTS

A typical image of a sphere 8-mm in diameter, embedded in gel phantom is shown in Figure 3. The center of sphere was located at the 50-mm depth from the irradiated surface, and its center was shifted 8-mm to

the left from the phantom's center. This model experiment was performed to test the sensitivity and resolution of our optoacoustic imaging system.

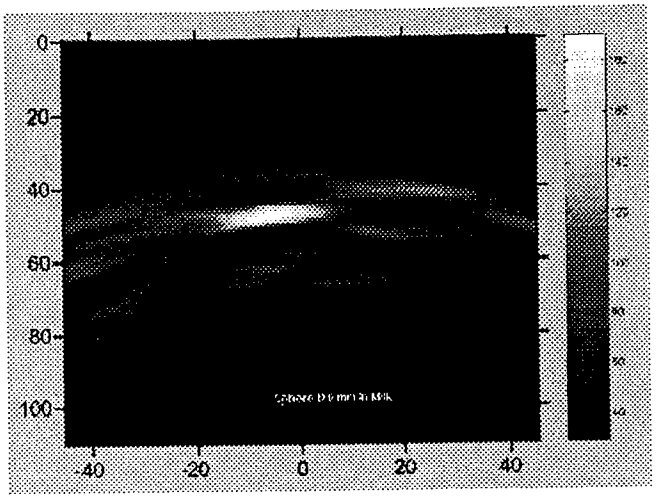

Figure 3. A 8-mm diameter gel sphere located at a depth of 5-cm in milky phantom resembling optical properties of the breast. Axes are scaled in millimeters. The optical contrast of the sphere above the background medium equals 5.

The top of Fig. 3 corresponds to the location of optical fibers (Y=0 mm), while bottom of this figure corresponds to the position of transducer array (Y=110 mm). The center of the transducer array was at the zero of X-axis. The opto-acoustic image in Fig. 3 represents the distribution of a product of thermo-acoustic efficiency, optical absorption coefficient and the absorbed laser energy. The brightest parts of the image correspond to the maximum values of this product. The sphere location and its vertical dimension accurately correspond to their real values. The lateral size of image is approximately 3 times larger than the sphere diameter. It demonstrates the limit of lateral resolution of the system. Five positions of illuminating fiber with 6-mm increment were employed to collect data for this image reconstruction.

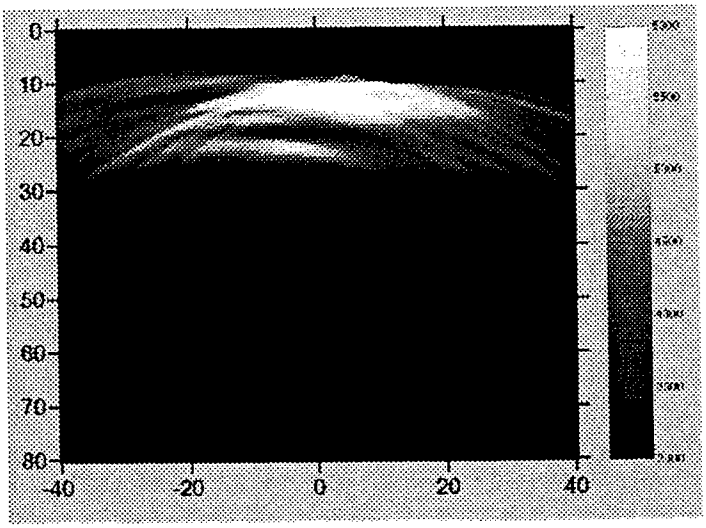

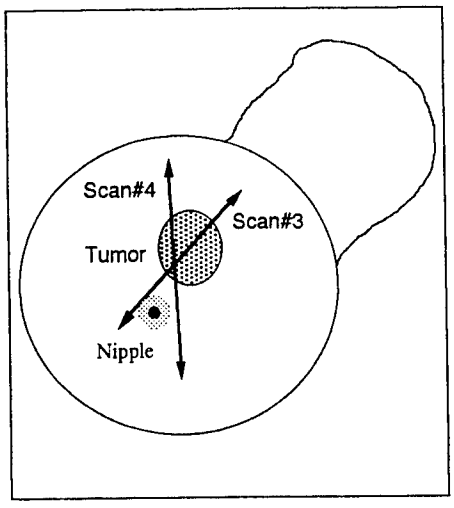

Figure 4. Opto-acoustic image of a large tumor. Scan #3. Patient 052291P.

Typical results of the clinical opto-acoustic imaging are presented in Figures 4 - 9.

The laser, the acoustic transducer array and the data acquisition system were placed on a cart. The cart provided means for fast transportation of the system to the frozen section room in Pathology Department where all measurements were performed.

The image of large well palpable tumor is shown in Fig. 4. Total of four opto-acoustic scans were made. The data for the image presented in Fig. 4 were obtained when the scan passed directly over the tumor (scan #3). Tumor position and direction of scans are shown in the diagram (on the right). Axes in Fig. 4 are scaled in millimeters. The top of the figure (Y = 0 mm) corresponds to the skin surface, while the transducer array was located on the bottom (Y = 80 mm). Two bright domains in Fig. 4 depict a two-lump tumor (a smaller lump was located underneath the larger lump. The full vertical size of this tumor could be determined as 16-18 mm. The depth of the tumor was found to be 10-12 mm from the skin surface. Spherical shadow arcs in the tumor image appeared due to the secondary lobes in the sensitivity diagram of the ultrasonic reception of the array transducer [29]. This type reception diagram represents the major limitation for the lateral resolution in our imaging system.

The temporal integral of the initial signal, detected by one of the transducers in array is shown in Fig. 5. Initial signal consists of the three components: short N-shaped signals generated by the small absorbing tumors, a lower-frequency smooth-rise exponential slope produced by the optical attenuation inside the tissue, and transducer reverberations detected after the end of useful part of the signal.

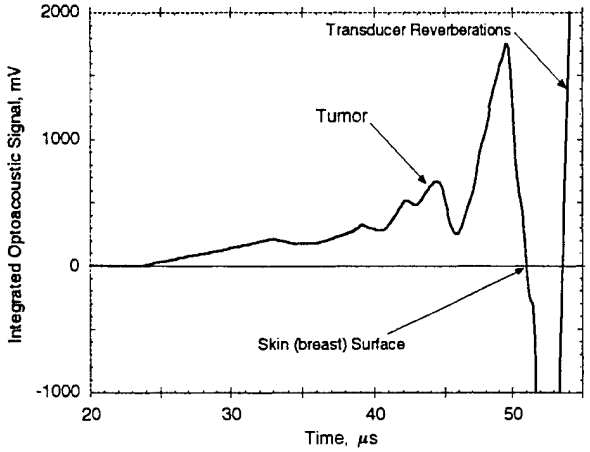

Figure 5. Integrated opto-acoustic signal profiles measured in the mastectomy specimen with tumor.

It is necessary to eliminate completely the low frequency signal component associated with homogeneous light attenuation inside the tissue, because it can significantly decrease the contrast in the process of image reconstruction. This was achieved in LOIS with a high-pass digital filtering using RC cells. Variation of the RC parameters and the number of cells permits a fine adjustment of the filter bandwidth and sharpness of this band profile.

High ultrasound frequencies that fall near the resonance frequency, f_{max}, of piezo-elements can induce significant reverberation in the transducer. Our transducers were designed to damp resonance frequencies and widen the range of detectable frequencies. Nevertheless, a strong reverberation takes place after the arrival of the signal from the surface of tissue. These reverberations do not affect the useful part of the opto-acoustic profile. Besides, it is convenient to employ the sharp gradient in the signal for automatic determination of the tissue surface. The position of maximum in the signal's derivative was considered as the position of the irradiated tissue surface. All data samples were cut off the signal after arrival of the surface signal. Nevertheless, the signal amplitude near the surface position remains high and could give rise to a bright area on images. To avoid the surface signal and to enhance the tumor image contrast the surface signal was also rejected.

The image of the same tumor but for another scan direction (scan#4) is shown in Fig. 6. This scan was made aside the tumor center. As a result, the depth of tumor image is slightly increased (14 –15 mm) and its vertical size is decreased (13-14 mm) compared with Fig. 4.

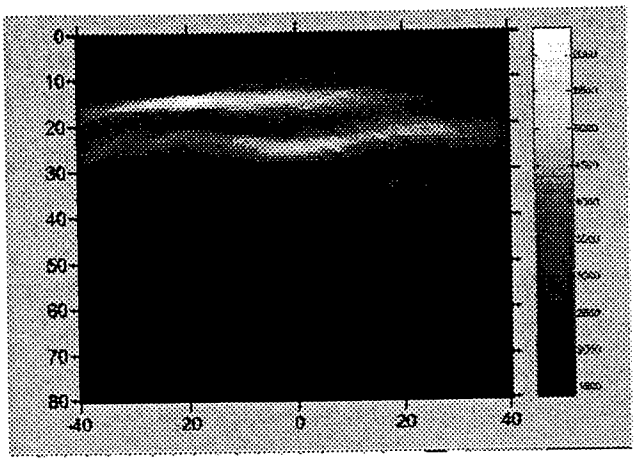

Figure 6. Image of tumor. Scan #4. UTMB Patient #052291P.

The main tumor lump (the brightest part on the image) is shifted towards the edge of the transducer array. At the depth of 40 mm a layer of blood on the surface of the transducer buffer is visualized. Blood was mixed with water and this solution was accumulated at the surface of the film covered the transducer buffer. The light absorption in this layer resulted in additional acoustic signal and this layer was imaged. The depth of this layer of diluted blood was relatively large (40 mm from the illuminating surface) and the blood concentration was weak. Thus, the visualization of this layer demonstrated high sensitivity of LOIS. As it was mentioned earlier the tumor depicted in Fig. 4, and Fig. 5 was large and it was detected and visualized as well by other imaging modalities (X-ray mammography, ultrasound, and MRI).

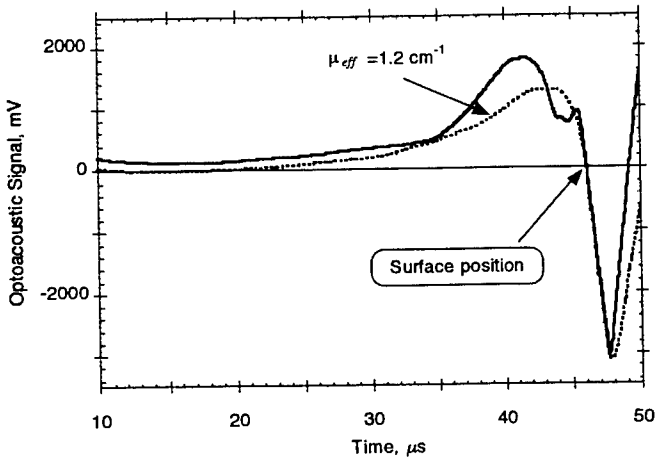

Figure 7. Opto-acoustic signal measured in normal breast tissue.

Fig. 7 presents acoustic signals exited in normal breast tissue. The acoustic signal (dotted curve) has a smooth shape without any peaks associated with additional light absorption. This form can be approximated by exponential function in order to determine the coefficient of optical attenuation in the breast. The optical attenuation of the normal breast tissues at the wavelength of 1064 nm was determined from Fig. 6 to be $\mu_{eff} = 1.2$

cm^{-1}. When the same tissue was illuminated through the skin layer (solid curve), an additional light scattering and attenuation in skin resulted in two-peak profile with increased amplitude of the acoustic profile.

The image of tumor attached to the surface of silicon implant is presented in MRI image and ultrasound image depicted in Fig. 8. The presence of implant complicated all imaging procedures, resulting in a very low contrast between the tumor and the implant. X-ray mammography (not shown) did not reveal any tumors. Both MRI and ultrasound depicted area suspicious to have a tumor (see a brighter area on the top surface of the implant). MRI system employed dynamic perfusion imaging with gadodiomide contrast agent that resulted in a better differentiation between tumor and the implant. However, the contrast between the tumor and surrounding tissues was not sufficient to make pathological conclusions. A biopsy performed following imaging demonstrated the presence of malignant cells in the suspicious area on implant surface.

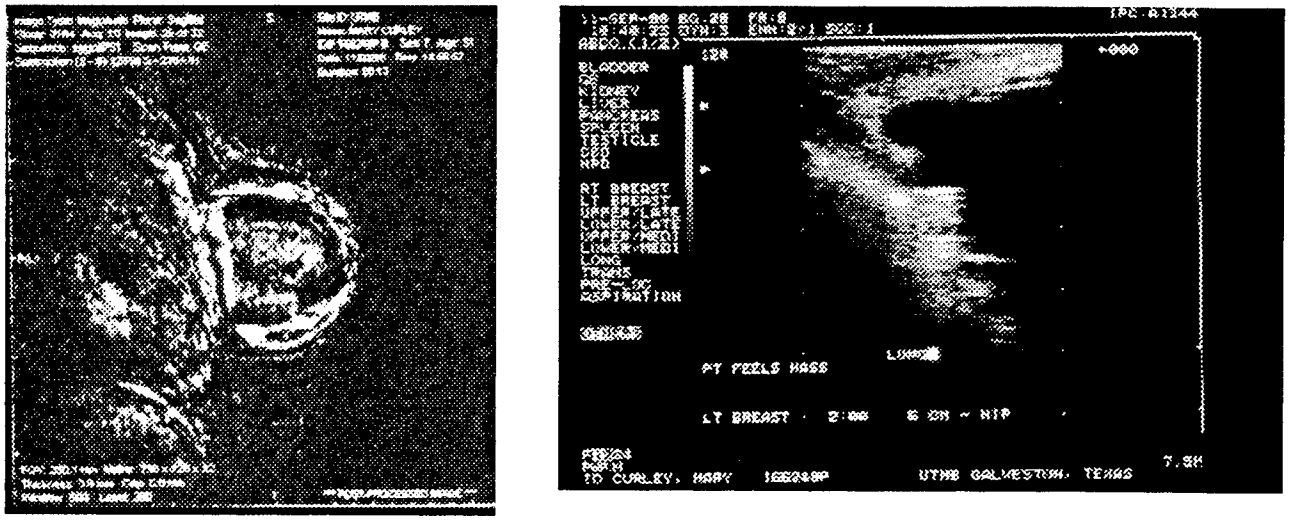

Figure 8. Differential MRI image of the breast with tumor (left, 1 minute after contrast minus pre-contrast), and Ultrasound image of the same breast, employing 7.5 MHz transducer.

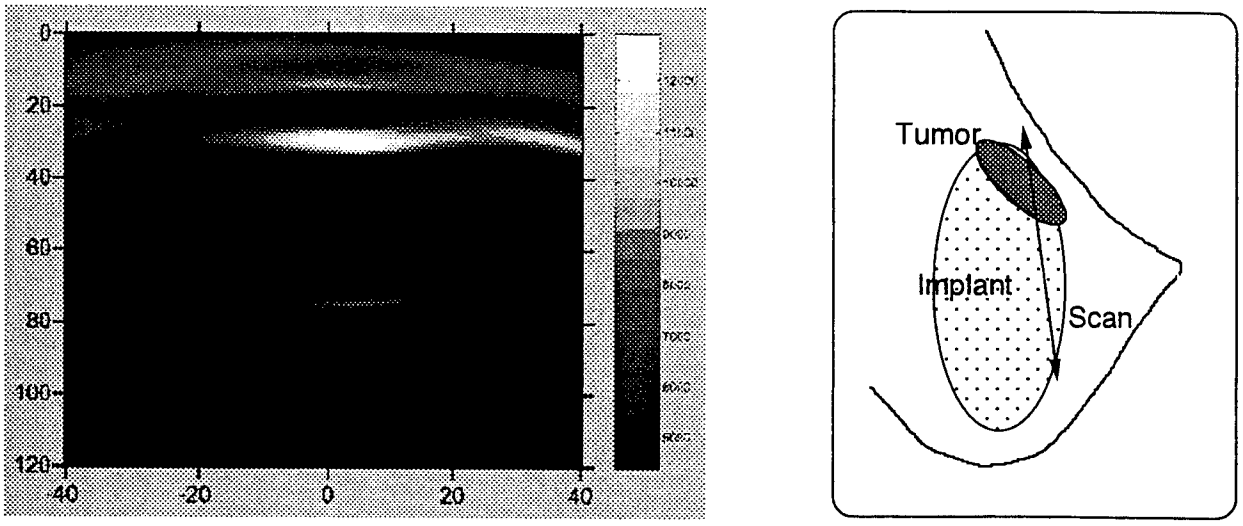

Figure 9. Tumor on the implant surface. UTMB Patient #166248P.

The corresponding opto-acoustic image is shown in Figure 9. The initial raw data for this image reconstruction were acquired during the scan shown in the diagram (to the right from the image). The implant was about 40 mm in thickness. The tumor (bright domain at the depth of about 30-mm from the skin surface) was detected near the top edge of implant. It is important to note that the tumor location on the opto-acoustic image differs from that on the MRI image to the factors influencing imaging of mastectomy specimen, i.e. (1) different shape and dimensions of the breast *in vivo* and after surgical excision, and (2) shifted position of the mastectomy specimen between the fiber and the transducer array compared with the natural position. The area where the enhanced light absorption was found had 5-7 mm thickness. Some blood drained to the transducer buffer surface (at the depth of approximately 75 mm) and mixed with water resulted in a visible mark on the image. The opto-acoustic tissue contrast between the tumor and the surrounding tissue and the implant is significant. However, an enhanced contrast could result from distortion of breast structure and blood accumulation after the biopsy.

4. DISCUSSION

This comparative study demonstrated that the laser opto-acoustic imaging could provide images with substantially better contrast than x-ray mammography and ultrasound imaging in case of radiologically dense, acoustically homogenous, but optically inhomogeneous phantoms. Contrast and sensitivity are the two interdependent parameters. The higher the tissue contrast, the higher the sensitivity of the opto-acoustic system in detecting small tumors. Effective noise pressure could be determined from the following expression:

$$p'_N = \frac{2\rho_0 c_S f_{\max}}{g_{33}} \sqrt{\frac{4kT}{C_0}} \qquad (1)$$

where g_{33} is the piezoelectric modulus, f_{max} is the maximum detected ultrasound frequency, C_0 is the transducer capacity.

Figure 10 shows effective noise pressure as a function of the transducer capacity for gradually increasing width of detected ultrasonic frequencies.

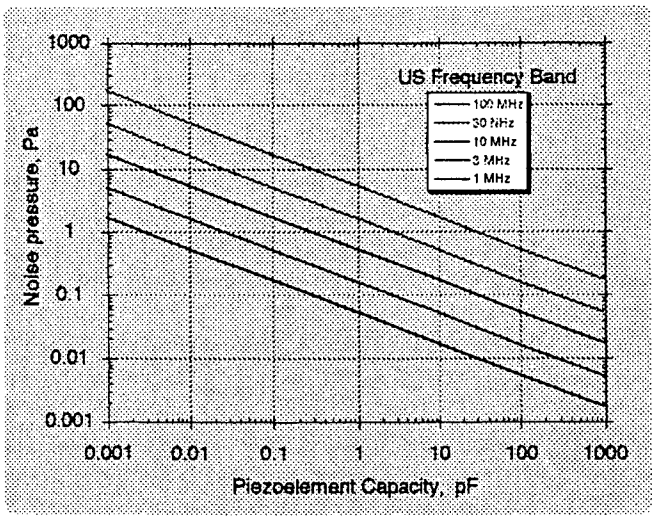

Figure 8. Effective noise pressure of the acoustic transducer.

A typical effective noise pressure is about 10 μbar=1 Pa for the acoustic transducers with capacity of about 10 pF.

The axial (in-depth) resolution of the pulsed opto-acoustic system operating under irradiation conditions of temporal pressure confinement is directly defined by the detection bandwidth of acoustic transducers. Two coherently emitting spherical acoustic sources with radius a_0 will be detected as separate objects if the space between their centers equals or greater than $\Delta z = 2a_0$. For correct detection of pulsed opto-acoustic waveform excited in a tumor with characteristic dimension a_0 it is necessary to detect opto-acoustic signals within a wide ultrasound frequency band equal approximately the ratio of the Cs/ a_0. Lateral resolution, δ, provided by an array of transducers can be estimated as a product of the angle of acceptance (numerical aperture) of the acoustic transducer and the total length of the transducer array.

5. CONCLUSION

The study performed with breast phantoms demonstrated capabilities of the laser opto-acoustic tomography in detection of small volumes with absorption equal to the absorption of 10% blood at the depth of up to 6 centimeters in phantoms resembling optical properties of breast tissues. Thus, the laser optoacoustic tomography has a potential for early detection of (small) breast tumors.

The first clinical prototype of the laser opto-acoustic imaging system was developed and tested on radical mastectomy specimen. Significant opto-acoustic contrast (~300%) between tumors and surrounding tissues was observed and exceeded the contrast of conventional imaging modalities. LOIS was capable of detection all and every tumor in mastectomy specimens. Because modern medical diagnostic techniques have limitations in detection of small tumors (with a volume of ≤ 4 mm^3) located at depths of 5-6 centimeters, the laser opto-acoustic imaging may occupy a significant niche in diagnosis of breast tumors, especially in radiologically dense and acoustically homogenous breasts.

ACKNOWLEDGEMENTS

This work was supported by the Advanced Technology Program of the Texas Higher Education Coordinating Board (grant # 004952-054), National Cancer Institute (grant #R29-CA80221) and US Army (grant #DAMD17-99-1-9404).

REFERENCES

1. S.H. Landis, T. Murray, S. Bolden, P.A. Wingo: Cancer Statistics 1999, *Cancer J. Clin.* 1999; **49**: 8-31.
2. W.L. Johnson: "Breast Cancer. Controversies in Management", Futura Publishing Co., Armonk, NY, 1994, pp. 293-339.
3. R. DeRossa: "Lifeline: Ultrasound", USA Today, April 15, 1996.
4. B.R. Friedman et al: "Principles of MRI", McGraw - Hill Information Services Co., New York-London-Paris, 1989.
5. W.G. Schreiber. G. Brix, M.V. Knopp, T. Hess, W.J. Lorenz: Improved visualization of breast lesions with gadolinium-enhanced magnetization transfer MR imaging, *Magnetic Resonance in Medicine* 1996; **35**(6):861-869.
6. K.A. Kvistad, S. Lundgren, H.E. Fjosne, E. Smenes, H.B. Smethurst, O. Haraldseth: Differentiating benign and malignant breast lesions with T2*-weighted first pass perfusion imaging, *Acta Radiologica* 1999; **40**(1): 45-51.
7. B.J. Tromberg, O. Coquoz, J.B. Fishkin, E.R. Anderson, D. Pham, M. Brenner, L.O. Svaasand: Frequency-Domain Photon Migration (FDPM) Measurements of Normal and Malignant Cell and Tissue Optical Properties", In: *"OSA Trends in Optics and Photonics on Biomedical Optical Spectroscopy and Diagnostics"*, ed. by E. Sevic-Muraca and D. Benaron, (OSA, Washington, DC), 3, pp. 111-116, 1996. 0

8. J. Folkman: What is the evidence that tumors are angiogenesis dependent? *J. Natl. Cancer Inst.*, 1990; **82**(1): 4-6.
9. N. Weidner, J.P. Semple, W.R. Welch, and J. Folkman: Tumor angiogenesis and metastasis - correlation in invasive breast carcinoma, *New Engl. J. of Med.*, 324, pp. 1-7, 1991.
10. A.J. Welch, M.J.C. van Gemert: Optical-Thermal Response of Laser-Irradiated Tissue, eds. Plenum Press, NY, 1995.
11. S. Wray, M. Cope, D.T. Deply, J.S. Wyatt, and E.O.R. Reynolds. "Characterization of the near infrared absorption spectra of cytochrome aa_3 and hemoglobin for the non-invasive monitoring of cerebral oxygenation", *Biochim. et Biophys. Acta*, 1988; **933**: 184-192.
12. J. Kolzer, G. Mitic, J. Otto, and W. Zinth: Measurements of the optical properties of breast tissue using time resolved transillumination", *Proc. SPIE* 1994; **2326**: 143-152.
13. K. Suzuki, Y. Yamashita, K. Ohta, M. Kaneko, M. Yoshida, and B. Chance. "Quantitative measurement of optical parameters in normal breasts using time-resolved spectroscopy: *in vivo* results of 30 Japanese women", *J. Biomed. Optics*, 1996; **3**: 330-334.
14. A.A. Oraevsky, S.L. Jacques, F.K. Tittel: Determination of tissue optical properties by time-resolved detection of laser-induced stress waves. *Proc. SPIE* 1993; **1882**: 86-101.
15. A.A. Oraevsky, S.L. Jacques, R.O. Esenaliev, F.K.Tittel: Laser based optoacoustic imaging in biological tissues, *Proc. SPIE* 1994; **2134A**: 122-128
16. R.A. Kruger, P. Liu: Photoacoustic ultrasound: Pulse production and detection in 0.5% Liposyn, *Medical Physics*, 1994; **21**(7): 1179-1184.
17. A.A. Oraevsky, R.O. Esenaliev, S.L. Jacques, F.K. Tittel, and D. Medina. "Breast Cancer Diagnostics by Laser Opto-Acoustic Tomography", *OSA Trends in Optics and Photonics on Advances in Optical Imaging and Photon Migration,"* R.R. Alfano and J.G. Fujimoto, eds. (OSA, Washington, DC), 2, pp. 316-321, 1996.
18. A.A Oraevsky, R.O. Esenaliev, S.L. Jacques, and F.K. Tittel. "Laser Opto-Acoustic Tomography for medical diagnostics: principles", *Proc. SPIE* 1996; **2676**: 22-31.
19. R.O. Esenaliev, F.K. Tittel, S.L. Thomsen, B. Fornage, C. Stelling, A.A. Karabutov, and A.A. Oraevsky: Laser optoacoustic imaging for breast cancer diagnostics: Limit of detection and comparison with X-ray and ultrasound imaging, *Proc. SPIE* 1997; **2979**: 71-82.
20. R.O. Esenaliev, A.A. Oraevsky, S.L. Jacques, and F.K Tittel. "Laser opto-acoustic tomography for medical diagnostics: Experiments on biological tissues", *Proc. SPIE* 1996; **2676**: 84-90.
21. A.A. Oraevsky, R.O. Esenaliev, S. L. Jacques, and F.K. Tittel. "Lateral and z-axial resolution in laser optoacoustic imaging with ultrasonic transducers", *Proc. SPIE*, 1995; **2389**: 198-208.
22. R.O. Esenaliev, H. Alma, F.K. Tittel, A.A. Oraevsky: Axial resolution of laser optoacoustic imaging: influence of acoustic diffraction, *Proc. SPIE* 1998; **3254**: 294-306.
23. Oraevsky, A.A., S.L. Jacques, F.K. Tittel: Measurement of tissue optical properties by time-resolved detection of laser-induced transient stress, *Applied Optics*, 1997; **36**(1): 402-415.
24. S.A. Goss, R.L. Johnston, and F. Dunn. Comprehensive compilation of empirical ultrasonic properties of mammalian tissues, *J. Acoust. Soc. Am.*. 1978; **64**(2): 423-457.
25. F.A. Duck, "*Physical properties of tissue: A comprehensive reference book*", Academic Press, San Diego, 1990.
26. A.A. Oraevsky, S.L. Jacques, R.O. Esenaliev, and F.K. Tittel: Time-Resolved Optoacoustic Imaging in Layered Biological Tissues, In: *"OSA Proceedings on Advances in Optical Imaging and Photon Migration"* , ed. by R. R. Alfano, Academic Press, 21, pp. 161-165, 1994.
27. A.A. Oraevsky, R.O. Esenaliev, A.A. Karabutov: Laser optoacoustic tomography of layered tissues: signal processing, *Proc. SPIE* 1997; **2979**: 59-70.
28. A.A. Karabutov, N.B. Podymova, V.S. Letokhov. Time-resolved laser optoacoustic tomography of inhomogeneous media. *Appl. Phys. B* 1996; **63**: 545-563.
29. A.A. Oraevsky, V.G. Andreev, A.K. Karabutov, R.O. Esenaliev: Two-dimensional opto-acoustic tomography, transducer array and image reconstruction algorithm, *Proc. SPIE* 1999; **3601**A: 28.
30. American National Standard for Safe Use of Lasers", ANSI Z136.1 and Z136.3, 1993.

Ultimate Sensitivity of Time-Resolved Opto-Acoustic Detection

Alexander Oraevsky and Alexander Karabutov

Optoacoustic Imaging and Spectroscopy Laboratory, CBME,
University of Texas Medical Branch, Galveston, Texas 77555-0456

ABSTRACT

The major limitation in sensitivity of the optical tomography is associated with strong optical attenuation in human tissues. Opto-Acoustic Tomography overcomes this limitation utilizing detection of acoustic waves instead of detection of transmitted photons. Exceptional sensitivity of the opto-acoustic tomography allows early detection of small tumors located deep in human tissues, such as breast. This paper demonstrates that an optimally designed opto-acoustic imaging system can detect early 1-mm tumors with minimal blood content of only 7% at the depth of up to 7-cm within the breast attenuating laser irradiation 3.3 times per each 1-cm of its depth. A theoretical consideration of the ultimate sensitivity of piezo-detection in a wide ultrasonic frequency band is developed. The detection sensitivity is presented as a function of the ultrasonic frequency, tumor dimensions and optical absorption coefficient. Comparative analysis of piezo and optical interferometric detection of opto-acoustic transients is presented. The theoretical models of piezodetection were developed for the open-circuit and short-circuit schemes of operation. The ultimate sensitivity limited by thermal noise of electric capacitor of the piezo-element was estimated. It was shown that the limit of detection depends on the frequency band, the electric capacity of the transducer and the speed of sound in the piezo-element. Comparative analysis of various piezo-materials was made from the point of view of their utility for sensitive opto-acoustic detection.

Keywords: piezoelectric transducer, optical vibrometer, opto-acoustic imaging

1. INTRODUCTION

Advantages of the opto-acoustic imaging for characterization of optically heterogeneous tissue structures with high spatial resolution were demonstrated over the past several years [1-16]. One of the major merits of the opto-acoustic imaging is high sensitivity in detecting variations of laser-induced temperature or corresponding pressure. Unique characteristics of optoacoustics found utility in various medical applications, including detection of early cancer [7-11], monitoring therapeutic effects of lasers in tissues [12,13], measuring tissue properties and molecular content [1,14-16]. Optimal design and development of optoacoustic imaging and monitoring systems requires, first of all, comprehensive analysis of capabilities and limitations in detection of wide-band ultrasonic transients.

There are two general modalities that may be used for conversion of wide-band acoustic waves (mechanical displacement) into electronic signal: piezoelectric transducers [5,17-19] and optical interferometers and deflectors [20-22]. Noncontact nature of laser generation of ultrasound makes it attractive to develop fully noncontact opto-acoustic tomography and laser ultrasound evaluation systems employing optical methods of detection of acoustic transients. However, surface roughness (especially in skin and other uneven media) strongly compromises sensitivity of optical detection. The use any contact means for surface smoothing removes major advantage of noncontact optical methods relative to the contact piezoelectric detection. Therefore, the main attention is drawn in this paper to the piezoelectric detection of acoustic waves. The most sensitive acoustic detectors utilize resonance of physical dimensions and ultrasound wave to be detected. The product of sensitivity and the bandwidth is constant defined by properties of the detector. Therefore, detection within a narrow frequency band is the most sensitive. The sensitivity goes down simultaneously with widening of the ultrasound detection band. In order to account for the fact that sensitivity of acoustic transducer depends on the range and the bandwidth of ultrasound detection, one should consider the bandwidth-specific sensitivity of the ultrasonic detector.

The aim of this paper is to describe ultimate sensitivity of detection of acoustic waves in the entire ultrasonic frequency band from 20kHz to 200 MHz and to compare piezoelectric transducers versus optical interferometry as means for detecting transient ultrasonic signals induced in tissue with laser pulses. It is logical to divide all applications of the opto-acoustic imaging in three groups according to the required bandwidth of ultrasound detection: low, intermediate and high, (1) 20 kHz to 2 MHz, (2) 1 MHz to 20 MHz, and (3) 1 MHz to 200 MHz.

* Correspondence: email: alexander.oraevsky@utmb.edu, http://www2.utmb.edu/cbme/optoacoustic_imaging_&_spec.htm, phone: 1-409-772-8348

In *Biomedical Optoacoustics*, Alexander A. Oraevsky, Editor,
Proceedings of SPIE Vol. 3916 (2000) • 1605-7422/00/$15.00

The first group includes imaging and monitoring of tumors, blood vessels and other tissues located at the depth of up to 10 cm. Substantial depth of imaging prohibits the use of high ultrasound frequencies due to their strong attenuation in tissues. Therefore, spatial resolution is limited to sub-mm. The second group includes applications of tissue imaging at the depth of about 1-cm. These applications require a more detailed information of tissue structure and function, and therefore, employ detection of higher ultrasound frequencies in order to achieve resolution of several tens of microns. The third group includes applications of the opto-acoustic tomography in high resolution imaging of skin and mucosal surfaces of digestive tract, and in cell microscopy. Each group of applications and each corresponding range of detected ultrasound frequencies define a unique design of the opto-acoustic detection system.

2. ULTRASONIC SPECTRUM OF THE OPTO-ACOUSTIC SIGNAL

Opto-acoustic imaging of biological tissues utilizes absorption of optical energy by heterogeneous structures of tissue and materials and detection with temporal resolution of the wide-band ultrasound transients resulting from nonstationary thermal expansion [23]. The profile of acoustic wave emitted by a source with complex shape may be represented by the convolution of acoustic waves emitted by a number of small spherical sources. Therefore, below acoustic emission is described for a small optically absorbing sphere placed in nonabsorbing medium with thermomechanical properties similar to those of the sphere. Let us consider the case when laser-induced heat is evenly distributed over the spherical volume of $\frac{4\pi R_p^3}{3}$, where R_p is the radius of the sphere. Other types of radiation (such as microwave, IR or x-ray) and other shapes of absorbing object will not change our model qualitatively.

Acoustic pulse generated upon instant heating of the spherical volume can be expressed as in [24]:

$$p'(\tau = t - r/c_0) = \frac{1}{4\pi r}\frac{\beta c_0^2}{c_p}\frac{3E_{abs}}{2R_o^3}\begin{cases} -c_0\tau, & |c_0\tau| \le R_o; \\ 0, & |c_0\tau| \ge R_o; \end{cases} \qquad (1)$$

where $p'(\tau)$ is the pressure increse in ultrasonic wave propagating from the center of the sphere, β is the thermal expansion coefficient, C_P is the specific heat-capacity, E_{abs} is the optical energy absorbed by the sphere, r is the distance from the point of observation to the center of the spherical particle.

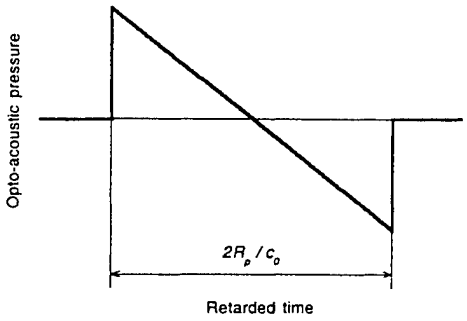

Figure 1. Typical N-shaped laser-induced acoustic profile of from a small absorbing sphere with radium R_p.

The opto-acoustic profile has an N-shape profile with traingle compression phase followed by the antisimmetric tension phase (see Figure 1). The total duration of the opto-acoustic signal is defined by the time of sound propagation along the diameter of the sphere. Since we consider the bandwidth specific sensitivity of the opto-acoustic system, let us consider

the spectrum of the ultrasonic signal. The ultrasonic spectrum of the opto-acoustic signal (1) could be obtained taking Fourier transform of the signal's temporal profile.

$$p_{ac}(\omega) = \int_{-\infty}^{+\infty} p'(\tau)\exp(-i\omega\tau)d\tau \tag{2}$$

The resulting spectrum has the following form:

$$p_{ac}(\omega) \propto \frac{(\omega R_p / c_0)\cos(\omega R_p / c_0) - \sin(\omega R_p / c_0)}{(\omega R_p / c_0)^2} \tag{3}$$

where is the frequency of ultrasonic vibrations. The modulus of this spectrum is given in Figure 2 as a sequence of oscillations rapidly decreasing in their amplitude. Maximum of the ultrasonic emission spectrum is given by the frequency,

$$f_{\max} = 0.33\frac{c_o}{R_p} \tag{4}$$

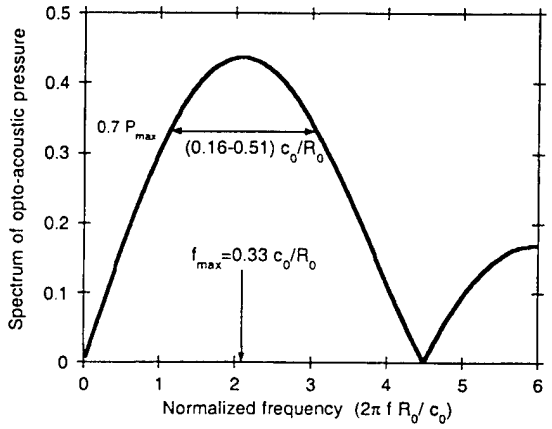

Figure 2. Fourier spectrum of acoustic emission from a small sphere as a function of ultrasonic frequencies.

The bandwidth of this spectrum is usually measured at the level of 0.707 or -3dB between $f_{lower} = 0.16\frac{c_o}{R_p}$ and $f_{upper} = 0.51\frac{c_o}{R_p}$. On the other hand, one has to take into account the presence of various absorbing objects in the laser-irradiated volume and detect all ultrasonic frequencies corresponding to variety of sphere dimensions from their minimum to maximum. Thus, wide band detectors in which the upper limit of the ultrasonic detection band exceeds the lower limit more than 10 times are required for correct opto-acoustic detection of laser-induced acoustic sources. Below we discuss noise level, signal-to-noise ratio (SNR) and sensitivity of this type wide-band acoustic trasnducers.

3. PIEZOELECTRIC DETECTION OF WIDE-BAND ULTRASONIC TRANSIENTS

There are two operation modes for wide band piezoelectric transducers: short circuit and open circuit (idling) [25]. The electrical circuits of the two modes of transducer operation are presented in Figures 3a and 3b.

The transducer operating in the short circuit has substantial thickness that is larger than the spatial width of the detected ultrasonic transient (Figure 3a). The transducer thickness limits the lower limit of detected ultrasonic frequencies and duration of the detection gate. An excessively big thickness of the piezoelement would (1) lead to a more prominent

acoustic diffraction at lower ultrasonic frequencies in the detected signal and (2) reduce the electric capacity to the value below the electric capacity of the electronic circuitry. It is difficult to design acoustic transducers operating in short-circuit mode for detection of opto-acoustic profiles longer than 1 μs. However, these transducers would be most optimal for detection of submicrosecond and nanosecond opto-acoustic signals. The upper limit of ultrasonic frequency is defined by the discharge time of the transducer capacity, C_T through the resistor, R. With low values of RC_T the ultrasonic detection band could reach several hundred MHz. The optimal value of the resistor R equals wave resistance of the electrical cable (50 to 200 Ohm).

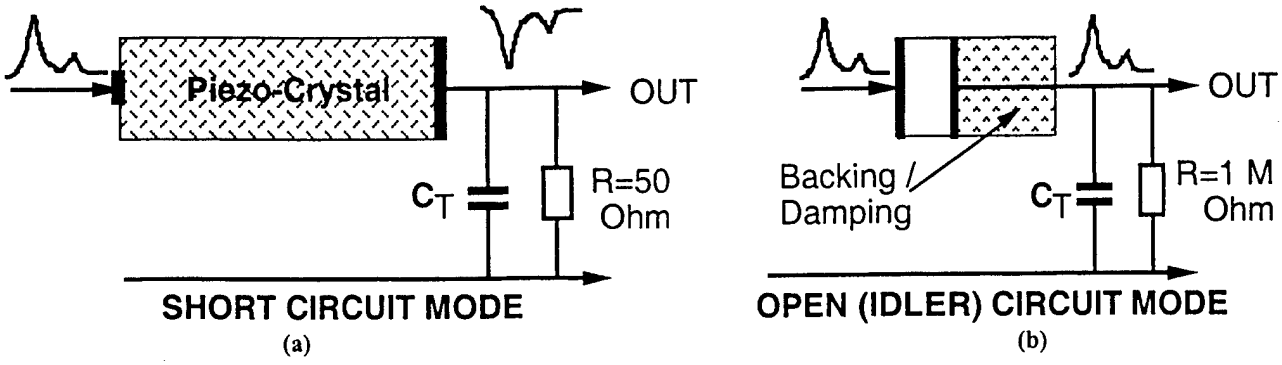

Figure 3. Electric circutry for the short (a) and idler (b) operation modes of the wide-band acoustic transducer.

In case of acoustic transducer operating in idler circuit mode (Figure 3b) it is necessary that the thickness of piezoelectric element be smaller than the acoustic wavelength detected in its upper ultrasonic frequency limit. The lower limit of detectable ultrasonic frequencies is defined by the discharge time of transducer electric capacity, C_T, through the input resistor of the electronic preamplifier, R. Therefore, it is desirable to design these acoustic transducers in one and the same housing with charge preamplifier. In order to design acoustic transducers operating in open (idler) circuit mode with very wide ultrasonic detection band (≥100 MHz), one have to employ very thin piezoelectric elements (thickness of just a few microns). Technocal difficulties are associated with flatness of the piezoelement and necessity for effective damping of high frequency resonances. Design of the backing layer acoustically matched with piezoelectric material for effecting damping of transducer resonances is one of the most important technical problems. These technical difficulties, however, are compemsated with a higher sensitivity of transducers operating in the open circuit mode. The sensitivity of open circuit transducers is about 50 times that of short circuit transducers due to longer holding of electric charge at the piezoelement.

3.1. Thermal noise in acoustic transducers operating in the open circuit mode.

Let us consider a thin piezoelectric layer placed in medium with ideally matching acoustic impedance and operated in open electric circuit (Fig.3b). The upper limit of detectable ultrasonic frequency determinde at the level of –3dB may be found from the following expression [26]:

$$f_{upper} = 0.44\frac{c_l}{l}, \tag{5}$$

where l is the thickness of piezoelectric element, c_l is the velocity of sound in piezoelectric material.

Therefore, minimal electric capacity of piezoelectric element is defined by the upper limit of ultrasonic detection band as:

$$C_T \geq \frac{2.3\varepsilon\varepsilon_0 A}{c_l} f_{upper}. \tag{6}$$

where A is the area of piezoelectric element, ε and ε_o are the dielectric constants of piezoelectric material and vacuum.

Formula (6) shows that the choice of piezoelectric material for wide-band acoustic transducers is affected not only by the dielectric permeability, as in case of resonance acoustic transducers, but also by the velocity of sound in piezoelectric material (in addition to upper ultrasonic frequency, f_{upper}).

For a transducer operating in the open circuit mode, the electrical conductivity of piezoelectric element substantailly exceeds the electric conductivity of the load resistor, i.e. the current through piezoelement is greater than the drain-current through the resistor. Therefore, the voltage due to thermal noise of the piezoelectric element of transducer can be found from thermal energy considerations (Neiquist formula) as:

$$\left\langle U_N^2 \right\rangle = \frac{4kT_0}{C_T}, \tag{7}$$

where k is the Boltsman constant, T_o is the temperature of piezoelement.

The voltage of piezoelectric effect is given by:

$$U_S = g_{33} l\, p', \tag{8}$$

where g is the piezoelectric pressure modulus of the transducer material. Sometimes, it is more convenient to use piezoelectric deformation modulus, $h_{33} = g_{33}\rho c_l^2$ for description of the piezoelectric sensitivity.

The pressure corresponding to the thermal noise voltage can be expressed combining formulas (7) and (8):

$$p_{\min} = \sqrt{\frac{9.2kT_0 f_{upper}}{c_l \varepsilon\varepsilon_0 g_{33}^2 A}} = \sqrt{\frac{9.2kT_o}{\eta_{ac} A}}. \tag{9}$$

The expression (9) indicates that the level of pressure minimally detectable with wide-band acoustic transducers operating in open circuit mode increases with increasing ultrasonic detection bandwidth. Here we introduced a parameter of piezoelectric element important for wide-band ultrasound detection and termed as «bandwidth-specific piezoelectric efficiency»:

$$\eta_{ac} = \frac{1}{f_{upper}} c_l \varepsilon\varepsilon_0 g_{33}^2, \tag{10}$$

This parameter defines optimal choice of the materizl for sensitive wide-band ultrasonic detection. Formula (10) shows that piezoelectric crystals with high velocity of sound are preferable in wide-band acoustic transducers, which represents not an obvious conclusion. The speed of sound in piezomaterial is not included in consideration of standard resonantly detecting ultrasonic transducers.

Table 1 lists the most important parameters of main piezoelectric materials that could be employed for wide-band ultrasonic detection. This table shows that Lithium niobate has the highest value of piezoelectric modulus. However, the highest possible piezoelectric efficiency for wide-band piezoelectric detection can be achieved with piezoceramics, such as PZT-5H. Somewhat lower sensitivity could be obtained with polyvinyldenefluoride (PVDF) or PVDF copolymers. Quartz and lithium niobate, materials widely used in piezoelectric inductry have significantly lower sensitivity for wide-band ultrasonic detection.

It is important to note that there could be other considerations, which may strongly influence advisability of various piezoelectric materials for the wide-band detection. The specific electrical capacity and the acoustic impedance of piezoelectric element are the two most significant parameters that have to be considered in addition to the bandwidth specific piezoelectric efficiency, η_{ac}.

Small specific capacity of transducer lower than several pF will decrease sensitivity of acoustic detection, because greater electrical capcity of electronic input circuits in preamplifier will shunt the transducer. This factor is the mose pronounced in detection of relatively low ultrasonic frequencies below 2 MHz. Therefore, the specific capacity of piezoelement defines its minimal thickness and area. PZT-5 and piezoceramic materails in general possess the highest linear capacity, and may be used in microminiature transducer designs.

The main disdvantage of piezoceramic materials for detection of wide-band ultrasonic transients (as well as piezoelectrics with crystal structure) is the occurrence of shear stress upon acoustic scattering at the boundaries of piezoelectric element. Transient shear waves result in strong effect on the transducer sensitivity within the ultrasonic detection band, and thus, in deformation of the detected opto-acoustic profile. This problem does not exist for piezoelectric

polymers, such as PVDF. Piezoelectric composite materials also allow effective damping of shear waves that might be generated in piezoceramics. Therefore, piezopolymers and PZT-epoxy composite materials certainly have noticeable advantage for use in transducers with ultrasonic bandwidth below 20 MHz. However, a great deal of difficulty in fabricating piezopolymers and composites with high quality flat surfaces makes them undesirable for transducers operating in ultrasonic frequency range above 20-30 MHz.

Table 1. Properties of various piezoelectric materials employed for wide-band ultrasound detection

Property / Material	Lithium Niobate	Quartz	PZT-5	PVDF
$\rho_o, 10^3\, kg/cm^3$	4.63	2.21	7.5	1.8
$c_l, 10^3\, m/s$	7.26	5.57	4.0	1.4
$\rho_o c_l, 10^6\, kg/m^2 s$	33.6	12.3	30	2.5
$g_{33}, Vm/N$	0.23	0.058	0.025	0.18
ε, dielectric permeability	29	4.55	1200	9.4
$\varepsilon\varepsilon_0 / c_l, pF/mm^2 MHz$	0.081	0.017	6.1	0.17
$c_l \varepsilon\varepsilon_0 g_{33}^2, 10^{-9}\, m^3/sN$	**0.99**	**0.75**	**27**	**3.8**
$h_{33}, 10^9\, N/C$	5.1	4.4	3.0	0.64
$\varepsilon\varepsilon_0 h_{33}^2, 10^9\, J/m^3$	**6.7**	**0.78**	**95**	**0.034**

Therefore, application of easy-to-polish crystals of quartz and lithium niobate has significant technological merit in the ultrasonic frequency range above 30 MHz. Piezoceramic materials have very high absorption in the ultrasonic range above 20-30 MHz, and thus, not used in this ultrasonic frequency range. In contrast, piezoceramics is a dominating material for manufacturing transducers operating in MHz and sub-MHz ranges, especially microminiature transducers.

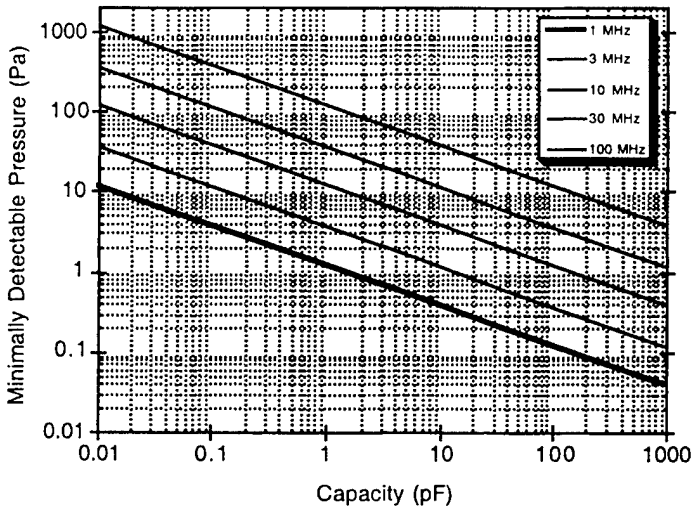

Figure 4. Acoustic pressure generated by thermal noise of acoustic transducer (operating in idler mode) as a function of its electric capacity presented for five different ultrasonics bands (upper curve for the bandwidth of 100 MHz).

Similarity of acoustic impedances of PVDF films and biological tissues makes PVDF preferable for design of continuously matching through acoustic tract. However, through matching is not as important for wide-band ultrasonic detection as concordance of acoustic impedances between piezoelement and backing of the transducer. Furthermore, acoustic pressure increases upon transmission of ultrasound wave from medium with lower acoustic impedance into the medium with higher acoustic impedance, thereby increasing sensitivity of transducer in measuring opto-acoustic pressure generated in the medium with lower acoustic impedance (such as biological tissue). Low acoustic impedance of polyvinylidenefluoride makes PVDF the material of choice for a number of applications in medical and biological sensing. Design of effective backing for PVDF transducers does not represent a great problem and makes detected opto-acoustic signals clear from reverberations within the piezoelement. For this reason, here we made quantitative estimates for wide-band ultrasonic transducers made of PVDF.

Minimally detectable pressure, p_{min}, is presented in Fig. 4 as a function of electric capacity, C_T, of piezoelement operating in open circuit mode. Taking into account that the the thermal noise voltage is proportional to the square root of the piezoelement capacity (see formula (7)). The electric capacity is inversely proportional to the thickness of piezoelement, and the thickness, in turn, is defined from the upper limit ultrasound frequency, then the minimally detectable pressure can be found from the following expression:

$$p_{\min} = \frac{4.6 f_{upper}}{g_{33} c_l} \sqrt{\frac{kT_0}{C_T}}, \tag{11}$$

Fig. 4 demonstrates that extremely low acoustic pressure measured in units of Pascale could be detected with transducers operating in a very wide frequency range of several tens MHz.

3.2. Detection of opto-acoustic signals with transducers operating in short circuit mode.

Correct (undisturbed) detection of opto-acoustic signals with transducers operating in short circuit mode is possible only within the temporal window equal the time of sound propagation along the thisckness of piezoelectric element. Electrical current through the piezoelement is proportional in this window to the vibrational velicity of the transducer front surface, while the rear surface stay still. Thus, detection of long opto-acoustic signals requires substantial thickness of the transducer piezoelemnt. The drawback of thick piezoelemnts is low electrical capacity and reduced sensitivity of transducer resulting from shunting effect of comparable electrical capacity of preamplifier and other electronic circutry of the transducer. On the other hand, due to the fact that resonance properties of the piezoelement (and reverberations) do not manifest themselves within this temporal window, the short circuit mode provides an even sensitivity characteriztics in a wide ultrasonic frequency range.

The range of detectable ultrasonic frequencies is defined in the short circuit mode by the time of electric discharge of piezoelement capacity through the load resistor. The spectral reasponse curve of transducer sensitivity can be presented in this case as:

$$|S| = \left(1 + (2\pi f R C_T)^2\right)^{-1/2}, \tag{12}$$

The corresponding bandwidth at the level of 0.7 Smax can be expressed as:

$$f_{upper} = \frac{0.16}{RC_T}, \tag{13}$$

As the electrical current through the piezoelement, I_{pe} in the short circuit mode is proportional to vibrational velocity, the expressions of Ohm and piezoelectric effect yield the following voltage at the load resistor:

$$U_T = R I_{pe} = R C_T g_{33} c_l p'. \tag{14}$$

The thermal noise is defined by the load resistor and could be found using consideration of Neiquist:

$$C_T U_T^2 = 4kT_0 R\Delta f = 1.1kT_o \tag{15}$$

where $\Delta f = \sqrt{3} f_{upper}$ is the ultrasonic detection bandwidth at the level of half-maximum.

Therefore, the voltage of thermal noise, which defines minimally detectable pressure,

$$p_{\min} = \frac{6.5 f_{upper}}{g_{33} c_l} \sqrt{\frac{kT_0}{C_T}} \tag{16}$$

is inversely proportional to the piezoelement capacity. The expression (16) found from combining formulas (13), (14), and (15) closely resembles that for the open circuit mode (11).

The short circuit mode is justified for detection of short opto-acoustic sisgnals with nanosecond temporal resolution. Crystal piezomaterials, such as lithium niobate and quartz are the materials of choise for the wide-band transducers operating in the short circuit mode. An important characteristics of these piezoelectric crystals for transducers operating in high ultrasonic frequency range (up to several hundred MHz) are associated with low attenuation of acoustic waves, negligible compared with piezoceramic materials. Furthermore, required flatness and parallelizm of piezoelement surfaces make crystal piezoelectrics much preferable for high frequency acoustic signals.

Furthermore, it is possible to enhance effectively the sensitivity of piezoelectric transducers relative to the pressure in media with relatively low acoustic impedance, such as biological tissue. This enhancement can be achieved upon transmission of ultrasonic waves from a medium with low acoustic impedance into the the medium with high acoustic impedance. Thickness of each layer is limited on one hand by the necessity to avoid acoustic diffraction (layers may not be made too thick) and on the other hand by resonances of low ultrasonic frequencies (layers may not be made too thin). Nevertheless, the pressure amplitude could be enhanced 3 –3.5 times in a system with three layers with gradually increasing acoustic impedance, so that each transmission increases pressure amplitude 1.5—1.8 times in the course of acoustic wave propagation through each of the two interfaces.

4. ULTIMATE SENSITIVITY OF OPTO-ACOUSTIC DETECTION

Let us estimate ultimate detection capability of wide-band opto-acoustic transducers described in Section 3 and applied for measurements of wide-band pressure transients described in Section 2. Here we calculate minimally detectable temperature-rise and correspondent volume increase in a small optically absorbing sphere embedded in optically attenuating medium with acoustic impedance matching that of the sphere. An optimal ultrasonic detection band for acoustic waves induced by laser pulses in this sphere is given by expression (4). The acoustic amplitude emitted by this sphere can be found from the expression (1), which could be also presented as:

$$p_{ac} = \rho_o c_s^2 \beta \Delta T \frac{R_p}{2r} \tag{17}$$

where ρ_o is the densitity of the sphere and the surrounding medium, and ΔT is the temperature-rise caused by absorption of laser pulses. The pressure increase measured at the distance r from the sphere is determined by an instant pressure increase in the heated sphere multiplied by a reducing factor equal to the ratio of the sphere radius and the distance to the measurement point, r. Additional factor 2 appears from the fact that thermoelastic pressure is devided equaly between two waves propagating outside from the sphere and insdie into the sphere. The rarefaction phase in the spherical acoustic wave could be explained as a compression wave propagating into the sphere and reflecting from the center with sign change.

For detection of a spherical acoustic wave with ultimate sensitivity, one needs to employ a spherical acoustic transducer (or array transducer with equivalent synthetic aperture) shaped to match the spherical phase front of the acoustic wave. The focus of such a transducer needs to match the location of the absorbing sphere. Therefore, the area of such transducer and the radius of its spherical curvature could be expressed as:

$$A = \Omega r^2 \tag{18}$$

Bringing together the expressions (17), (18), (4) and (9) one can get the following equation for minimally detectable temperature increase in laser-irradiated sphere:

$$\Delta T_{\min} = \frac{4.3}{\beta}\sqrt{\frac{kT_0}{\varepsilon\varepsilon_0 h^2 \Omega R_p^3}} \tag{19}$$

where h is the piezoelectric deformation modulus, Ω is the solid angle covered by the acoustic transducer and measured from the focal point located in the center of the absorbing sphere.

Formula (19) shows that minimally detectable temperature is inversely proportional to the square root of the volume absorbing laser energy. Thus, an ultimate sensitivity of the opto-acoustic detection has limitation associated with physical dimensions of detected object. Any increase in spatial resolution of the optoacoustic imaging will unavoidably result in an increase of minimally detectable pressure or temperature.

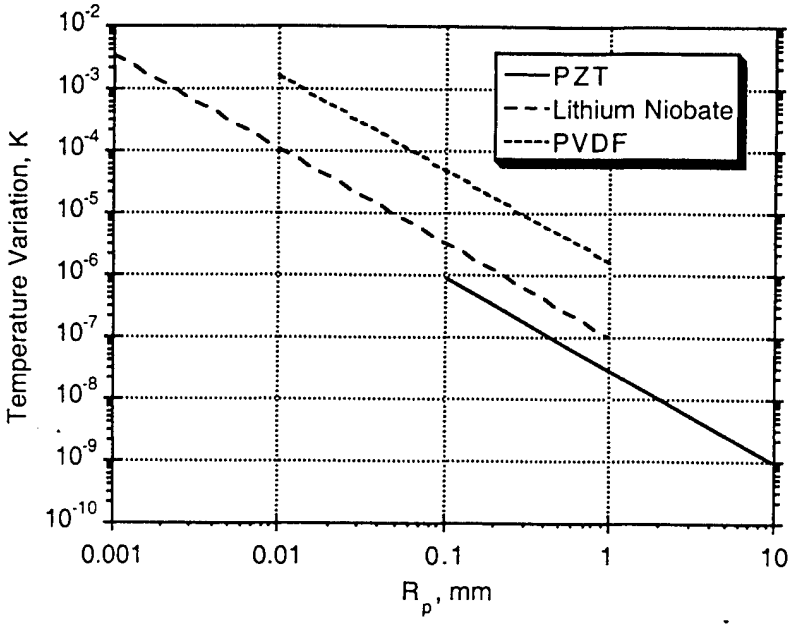

Figure 5. Minimally detectable temperature jump in tissue as a function of characteristic dimensions of absorbing sphere for three piezoelectric materails. Curve for each piezoelectric material is presented in an optimal ultrasonic frequency range.

Figure 5 depicts minimal detectable temperature generated in the volume of a small absorbing sphere as a function of the sphere radius for wide-band acoustic transducers made of various piezoelectric materials. Maximum sensitivity could be obtained with piezoceramic transducers. Lithium niobate possesses somewhat lower sensitivity, and the lowest sensitivity can be achieved with piezopolymers, such as PVDF. However, even with PVDF transducers it is possible to detect impressively low temperature jumps in biological tissues that usually possess substantial values of thermoelastic expansion coefficient ($\beta \approx (2-10)\bullet 10^{-4}[1/K]$). Fig. 5 demonstrates that with optimal design of the spherical piezoelectric transducer (solid angle of detection $\Omega = 1$), it is possible to detect a temperature increase of only ΔT~1-2 μK in a spherical tissue volume of about 1-mm^3, which permits application of low laser irradiation fluences significantly below safe levels of laser irradiation of human tissue [27].

5. DISCUSSION OF POSSIBLE APPLICATIONS

The major trade-off in opto-acoustic imaging is between sensitivity and spatial resolution. Therefore, various applications of the optoacoustic tomography require different piezoelectric transducers with ultrasonic detection bandwidth optimized for each application. One of the most prominent medical applications is the detection and characterization of small deeply located tumors in large human organs, such as breast or brain. Significant depth of some tumors (up to 6-7 cm from the surface) prohibits propagation of high frequency ultrasound to the acoustic transducer. Therefore, spatial resolution that

may be achieved is about 0.3-mm to 0.5-mm. However, the emphasis in deep opto-acoustic imaging could be made on high sensitivity in order to detect small (2-mm) tumors at the maximum possible depth.

Assuming that a small spherical tumor is relatively transparent for optical radiation, i.e. $\mu_a R_p < 1$, and laser pulses propagate to the tumor as spherical photon waves in tissue with effective optical attenuation, μ_{eff}, one can obtain an expression for the temperature increase inside spherical tumor located at a depth, z, within the irradiated tissue:

$$\Delta T = \frac{3\mu_a E(r = R_p)}{\rho_0 c_p} = \frac{3\mu_a E_0}{\rho_0 c_p} \frac{\exp(-\mu_{eff} z)}{\mu_{eff} z} \tag{20}$$

Substitution of (20) in (19) yields an equation that could be employed in practical estimates:

$$(\mu_{eff} z_{\max}) \exp(\mu_{eff} z_{\max}) = \frac{0.7\beta\mu_a E_0}{\rho_0 c_p} \sqrt{\frac{\varepsilon\varepsilon_0 h^2 \Omega R_p^3}{kT_0}} \tag{21}$$

Let us make our estimates using the following parameters, typical for a small breast carcinoma:

$\mu_a = 0.6\ cm^{-1} = 60\ m^{-1}$; $E_0 = 100\ mJ/cm^2 = 10^3\ J/m^2$; $\Omega = 1$; $\beta = 10^{-3}\ K^{-1}$; $\rho_0 c_p = 4*10^6\ J/m^3 K$

The piezoelectric transducer made of PZT-5 ceramics has not only high piezoelectric pressure modulus, but also substantial acoustic impedance, ρc_l, which results in two times greater pressure amplitude compared with the pressure in tissue. The combination of all parameters used yield the following piezoelectric efficiency: $\varepsilon\varepsilon_0 h^2 = 3.8*10^{11}\ J/m^3$, and therefore

$$(\mu_{eff} z_{\max}) \exp(\mu_{eff} z_{\max}) = 3.2*10^6 * (R[mm])^{3/2} \tag{22}$$

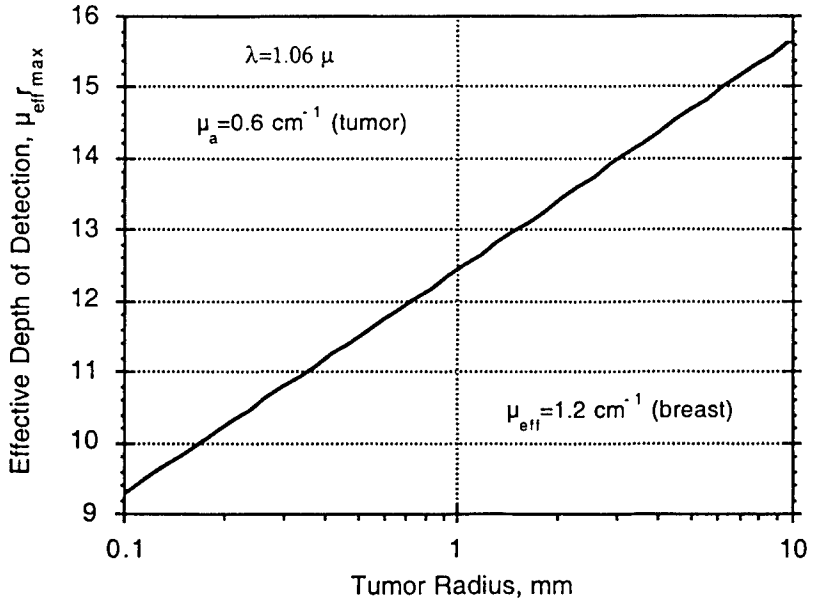

Figure 6. Maximum depth of a small tumor detection with opto-acoustic imaging performed in forward mode.

Maximum depth of opto-acoustic detection for a small tumors in the breast is shown in Fig. 6 as a function of tumor radius. This figure demonstrates that a tumor with characteristic dimension of about 1-mm may potentially be detected at the

depth of 12-13 effective optical penetration depths. For the breast irradiated with laser pulses at the wavelength of 1064-nm this yields physical depth of 10-12 cm.

The estimate presented in Fig. 6 was made for piezoelectric transducers made of piezoceramic materail, PZT-5. On the other hand, novel piezocomposite materails might provide even greater sensitivity resulting from enhanced deformation of piezoelements with equal diameter and thickness in response to pressure waves. The piezocomposite materials may open additional capabilities in opto-acoustic tomography and other applications of time-resolved opto-acoustics.

6. CONCLUSION

Optimal design of wide-band piezoelectric transducers permits realization of transducer specifications close to theoretical limit. Ultimate sensitivity of wide-band ultrasonic detection in acoustic transducer operating as capacitor is limited by its thermal noise. The thermal noise decreases as a square root of increasing transducer capacitance and decreases linearly with decreasing ultrasonic detection bandwidth. The parameter, which defines optimal design of the transducer, was determined in this paper and called the bandwidth specific piezoelectric efficiency, η_{ac} (see formula (10)). This parameter includes the detection bandwidth, the piezoelectric modulus, and the speed of sound in the piezoelectric material. Geometrical parameters of the piezoelectric element are also important, as they define transducer capacity and spatial resolution of the opto-acoustic imaging. Consideration of the entire complex set of parameters that define sensitivity of wide-band piezoelectric detection, we determined three piezoelectric materials that work best in one of the three ranges of wide-band ultrasonic detection employed in opto-acoustic tomography:

Piezoelectric Material	Ultrasonic Frequency Range	Comments
Lithium Niobate, LiNbO3	1 MHz to 200 MHz	low frequency elements too thick
Piezoelectric Ceramics, PZT-5	20 kHz to 20 MHz	high frequency absorption too high
Polyvinyldenefluoride, PVDF	1 MHz to 80 MHz	high frequency elements too thin

Novel laser opto-acoustic imaging systems utilizing wide-band ultrasonic transducers have a great potential in detecting such small features and tissue structures in biological tissue as early cancer. The tissue contrast in opto-acoustic tomography is defined by the laser wavelength employed and differences in tissue optical properties. Therefore, proper choice of the wavelength of laser irradiation is an important factor in realization of ultimate parameters of the opto-acoustic tomography. However, the most important factors are associated with design of opto-acoustic transducers, which includes choice of piezoelectric material, ultrasonic detection bandwidth, and electronic circuitry of charge preamplifiers.

ACKNOWLEDGEMENTS

This work was supported by the Advanced Technology Program of the Texas Higher Education Coordinating Board (grant # 004952-054), National Cancer Institute (grant #R29-CA80221) and US Army (grant #DAMD17-99-1-9404).

REFERENCES

1. A.A. Oraevsky, S.L. Jacques, F.K. Tittel: Determination of tissue optical properties by time-resolved detection of laser-induced stress waves. *Proc. SPIE* 1993; **1882**: 86-101.
2. A.A. Oraevsky, S.L. Jacques, R.O. Esenaliev, F.K.Tittel: Laser based optoacoustic imaging in biological tissues, *Proc. SPIE* 1994; **2134A**: 122-128
3. A.A. Oraevsky, S.L. Jacques, R.O. Esenaliev, and F.K. Tittel. "Time-Resolved Optoacoustic Imaging in Layered Biological Tissues", In: "OSA Proceedings on Advances in Optical Imaging and Photon Migration" , ed. by R. R. Alfano, Academic Press, **21**, pp. 161-165, 1994
4. R.A. Kruger, P. Liu, "Photoacoustic ultrasound: Pulse production and detection in 0.5% Liposyn", *Medical Physics*, Vol. **21**(7), pp. 1179-1184, 1994.
5. A.A. Oraevsky, R.O Esenaliev, S.L. Jacques, S. Thomsen, F.K. Tittel: Lateral and z-axial resolution in laser optoacoustic imaging with ultrasonic transducers, Proc. SPIE 1995; **2389**: 198-208.
6. A.A. Oraevsky, R.O. Esenaliev, S.L. Jacques, and F.K. Tittel. "Laser Opto-Acoustic Tomography for medical diagnostics: principles", *Proc. SPIE* **2676**, pp. 22-31, 1996.

7. R.A. Kruger, P. Liu, Y.R. Fang, R. Appledorn: Photoacoustic ultrasound: PAUS reconstruction tomography", *Medical Physics*, 1995; **22**: 1605-1609.
8. A.A. Oraevsky, R.O. Esenaliev, S.L. Jacques, F.K. Tittel, D. Medina. "Breast cancer diagnostics by laser optoacoustic tomography", OSA Trends in Optics and Photonics on Advances in Optical Imaging and Photon Migration," R. Alfano & J. Fujimoto, eds. v.**2**, pp. 316-321, 1996.
9. R.O. Esenaliev, F.K. Tittel, S.L. Thomsen, B. Fornage, C. Stelling, A.A. Karabutov, and A.A. Oraevsky: Laser optoacoustic imaging for breast cancer diagnostics: Limit of detection and comparison with X-ray and ultrasound imaging, *Proc. SPIE* 1997; **2979**: 71-82.
10. A.A. Oraevsky, A.A. Karabutov, E.V. Savateeva, B. Bell, M. Motamedi, S.L. Thomsen, J. Pasricha: Optoacoustic detection of oral cancer: feasibility studies in hamster model of squamous cell carcinoma, *Proc. SPIE* 1999; **3597**: 385-396.
11. A.A. Oraevsky, V.A. Andreev, A.A. Karabutov, D.R. Fleming, Z. Gatalica, H. Singh, R. O. Esenaliev: Laser optoacoustic imaging of the breast: Detection of cancer angiogenesis, *Proc. SPIE* 1999, **3597**: 352-363.
12. S. Thomsen, H. Vijverberg, S.L. Jacques, A.A. Oraevsky: Optical properties of albino rat skin in vitro. Comparison of photoacoustic and integrating sphere measurement techniques, *Proc. SPIE* 1994; **2134**: 106-113
13. R.O. Esenaliev, A.A. Karabutov, M. Motamedi, A.A. Oraevsky: Real-time optoacoustic monitoring of photothermal laser-tissue interactions, *Proc. SPIE* 1999; 3601: 268-274.
14. A.A. Oraevsky, R.O. Esenaliev, S.L. Jacques, L.H. Wang, M. Ostermeier, F.K. Tittel: Laser Opto-Acoustic Imaging of turbid media: comparison of experimental results and Monte Carlo simulations, *Proc. SPIE* 1996; **2681**: 277-284.
15. A.A. Oraevsky, S.L. Jacques, F.K. Tittel: Measurement of tissue optical properties by time-resolved detection of laser-induced transient stress, *Applied Optics*, 1997; **36**(1): 402-415.
16. A.A. Karabutov, E.V. Savateeva, N.B. Podymova, A.A. Oraevsky: "Backward detection of laser-induced wide-band ultrasonic transients with optoacoustic transducer", *J. Appl. Phys*. 2000, **87**(4): 2003-2014.
17. A.A. Oraevsky: A nanosecond acoustic transducer with applications in laser medicine, *LEOS Newsletter* 1994; **8**(1): 6-8.
18. A.A. Karabutov, N.B. Podymova, V.S. Letokhov. Time-resolved laser optoacoustic tomography of inhomogeneous media. *Appl. Phys*. B 1996; **63**: 545-563.
19. CGA Hoelen, R. Pongers, G. Hamhuis, FFM de Mul, J. Greve: Photo-acoustic blood cell detection and imaging of blood vessels in phantom tissue, *Proc. SPIE*, 1998; **3196**: 142-153.
20. G. Paltauf, H. Schmidt-Kloiber, H. Guss: Optical detection of laser-induced stress waves for measurement of the light distribution in living tissue, *Proc. SPIE* 1996; **2923**: 127-135.
21. P.C. Beard, T.N. Mills: "Characterization of post mortem arterial tissue using time-resolved photoacoustic spectroscopy at 436, 461 and 532 nm", *Phys. Med. Biol.* **42**(1), 177-198 (1997).
22. G. Paltauf, H. Schmidt-Kloiber, H. Guss: "Light distribution measurements in absorbing materials by optical detection of laser-induced stress waves", Appl. Phys. Lett., **69**, 1526-1528 (1996).
23. V.E. Gusev and A.A. Karabutov: "Laser Opto-acoustics", AIP Press, New York, 1993.
24. G.J. Diebold and T. Sun. "Properties of optoacoustic waves in one, two, and three dimensions", *Acustica*, **80**, pp. 339-351, 1994.
25. G.S. Kino: "Acoustic waves. Devices, imaging, and analog signal processing", Prentice-Hall, Englewood Cliffs, 1987.
26. P.M. Morse, K.U. Ingard: "Theoretical Acoustics", McGraw-Hill Book Co., New York-Toronto-London, 1968
27. American National Standard for Safe Use of Lasers. ANSI Z136.1-1993.